Dinuclear Metallacycles with Single M−O(H)−M Bridges [M = Fe(II), Co(II), Ni(II), Cu(II)]: Effects of Large Bridging Angles on Structure and Antiferromagnetic Superexchange Interactions

Daniel L. Reger,*,[†] Andrea E. Pascui,[†] Elizabeth A. Foley,[†] Mark D. Smith,[†] Julia Jezierska,[‡] and Andrew Ozarowski*,[§]

[†]Department of Chemistry and Biochemistry, University of South Carolina, Columbia, South Carolina 29208, United States
[‡]Faculty of Chemistry, University of Wrocław, 50-383 Wrocław, Poland
[§]National High Magnetic Field Laboratory, Florida State University, Tallahassee, Florida 32310, United States

Ⓢ *Supporting Information*

ABSTRACT: The reactions of $M(ClO_4)_2 \cdot xH_2O$ and the ditopic ligands m-bis[bis(1-pyrazolyl)methyl]benzene (L_m) or m-bis[bis(3,5-dimethyl-1-pyrazolyl)methyl]benzene (L_m*) in the presence of triethylamine lead to the formation of monohydroxide-bridged, dinuclear metallacycles of the formula $[M_2(\mu\text{-OH})(\mu\text{-}L_m)_2](ClO_4)_3$ (M = Fe(II), Co(II), Cu(II)) or $[M_2(\mu\text{-OH})(\mu\text{-}L_m^*)_2](ClO_4)_3$ (M = Co(II), Ni(II), Cu(II)). With the exception of the complexes where the ligand is L_m and the metal is copper(II), all of these complexes have distorted trigonal bipyramidal geometry around the metal centers and unusual linear (L_m*) or nearly linear (L_m) M−O−M angles. For the two solvates of $[Cu_2(\mu\text{-OH})(\mu\text{-}L_m^*)_2](ClO_4)_3$, the Cu−O−Cu angles are significantly bent and the geometry about the metal is distorted square pyramidal. All of the copper(II) complexes have structural distortions expected for the pseudo-Jahn−Teller effect. The two cobalt(II) complexes show moderate antiferromagnetic coupling, $-J = 48−56$ cm^{-1}, whereas the copper(II) complexes show very strong antiferromagnetic coupling, $-J = 555−808$ cm^{-1}. The largest coupling is observed for $[Cu_2(\mu\text{-OH})(\mu\text{-}L_m^*)_2](ClO_4)_3$, the complex with a Cu−O−Cu angle of 180°, such that the exchange interaction is transmitted through the d_{z^2} and the oxygen s and p_x orbitals. The interaction decreases, but it is still significant, as the Cu−O−Cu angle decreases and the character of the metal orbital becomes increasingly $d_{x^2-y^2}$. These intermediate geometries and magnetic interactions lead to spin Hamiltonian parameters for the copper(II) complexes in the EPR spectra that have large E/D ratios and one g matrix component very close to 2. Density functional theory calculations were performed using the hybrid B3LYP functional in association with the TZVPP basis set, resulting in reasonable agreement with the experiments.
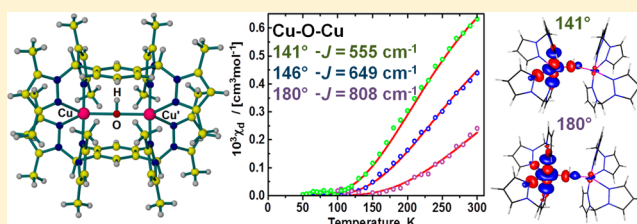
INTRODUCTION

Extensive efforts have been made to synthesize ligands designed to direct the organization of new metal complexes at the molecular and supramolecular level as a way to control different properties of the resulting materials.[1] One important class of ligands is based on poly(pyrazolyl)methane units, first introduced in 1970 by Trofimenko.[2] More recently, a series of second-generation tris(pyrazolyl)methane ligands, compounds with bulky groups substituted near the metal coordination site of the pyrazolyl nitrogen donor,[3] were synthesized. These ligands impact the coordination environment around the metal centers. This ligand family was then expanded to include third-generation poly(pyrazolyl)methane ligands, where the noncoordinating "back" position of the poly(pyrazolyl)methane unit is functionalized.[4] One class of third-generation ligands has several poly(pyrazolyl)methane units directionally oriented by linking with a designed central core. It has been shown that the number of poly(pyrazolyl)-methane groups as well as the type of linker influences the structure of the metal complexes.[4−6]

Of particular interest are the ditopic ligands L_m and L_m* (Scheme 1) that act as fixed, but not completely rigid ligands. The fixed *meta*-orientation of the bis(pyrazolyl)methane units

Scheme 1. Schematic Drawing of the Structure of L_m and L_m*

R = H L_m
R = Me L_m*
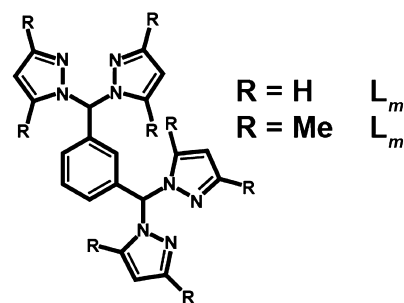
coupled with the free rotation around the arene−methine bond supports the formation of dinuclear metallacycles, such as $[Ag_2(\mu\text{-}L_m)_2](BF_4)_2$. These types of complexes have Ag···Ag nonbonding distances ranging from 4.1 to 5.3 Å.[4] With more highly charged metals (Mn(II), Fe(II), Co(II), Cu(II), and Zn(II)), dinuclear complexes still form, but abstraction of fluoride from the BF_4^- counterion, if present, leads to the formation of monobridged $[M_2(\mu\text{-}F)(\mu\text{-}L)_2]^{3+}$ complexes (L = L_m or L_m^*).[5,6] Interestingly, with M = Ni(II), Cd(II) difluoride-bridged complexes, $[M_2(\mu\text{-}F)_2(\mu\text{-}L_m)_2](BF_4)_2$ formed with the less bulky L_m,[4a,5] while the monofluoride-bridged species were isolated with L_m^*.[6] These complexes with the bulky L_m^* ligand nearly always have linear M−F−M bridging units, an arrangement that is uniquely important for magnetic studies.[7] We have previously reported detailed structural, magnetic, and EPR studies on the monofluoride-bridged complexes.[5,6] The complexes M = Mn(II), Fe(II), Co(II), and Ni(II) show moderate intramolecular antiferromagnetic exchange coupling between the two metal ions, while $[Cu_2(\mu\text{-}F)_2(\mu\text{-}L_m^*)_2](BF_4)_2$ shows strong antiferromagnetic coupling, $-J = 322$ cm^{-1}.[6]

Here we report the syntheses and characterization of analogous complexes with *bridging hydroxide* rather than fluoride, $[M_2(\mu\text{-}OH)(\mu\text{-}L)_2](ClO_4)_3$ (L_m: M = Fe(II), Co(II), Cu(II); L_m^*: M = Co(II), Ni(II), Cu(II)). Complexes containing a bridging hydroxide group are particularly important because this arrangement is frequently observed in biological systems.[8] The uniqueness of this linear or nearly linear bridged system allows us, for the first time, to maintain the overall structure relatively constant while altering a single structural feature of the complexes through selective modification of the bridging group (F$^-$ vs OH$^-$), the divalent metal ion, and/or the ligand (L_m vs L_m^*). Reported are detailed structural, magnetic, and EPR studies, supported by DFT calculations, of these monohydroxide-bridged complexes, with focus on the strength of the superexchange interactions. Part of this work has been communicated previously.[6b]

■ EXPERIMENTAL SECTION

General Considerations. For the synthesis of the hydroxide-bridged compounds, standard Schlenk techniques were used. The solvents were not dried prior to use, except for compound **1**, $[Fe_2(\mu\text{-}OH)(\mu\text{-}L_m)_2](ClO_4)_3$. The ligands L_m[4a] and L_m^*[6] were prepared following reported procedures. All other chemicals were purchased from Sigma-Aldrich or Strem Chemicals and used as received.

Crystals used for elemental analysis and mass spectrometry were removed from the mother liquor, rinsed with ether, and dried under vacuum, a process that removes the solvent of crystallization, if present. Mass spectrometric measurements were obtained on a MicroMass QTOF spectrometer in an acid-free environment. For all reported peaks, the isotopic patterns match those calculated for the assignment. Elemental analyses were performed on vacuum-dried samples by Robertson Microlit Laboratories (Ledgewood, NJ, USA).

High-field, high-frequency EPR spectra at temperatures ranging from ca. 6 to 290 K were recorded on a home-built spectrometer at the EMR facility of the NHMFL.[9] The instrument is a transmission-type device in which microwaves are propagated in cylindrical lightpipes. The microwaves were generated by a phase-locked Virginia Diodes source generating frequency of 13 ± 1 GHz and producing its harmonics, of which the 2nd, 4h, 6th, 8th, 16th, 24th, and 32nd were available. A superconducting magnet (Oxford Instruments) capable of reaching a field of 17 T was employed. The powder samples were not constrained and showed no magnetic torquing at high magnetic fields.

Magnetic susceptibility measurements over the temperature range 1.8−300 K were performed at a magnetic field of 0.5 T using a Quantum Design SQUID MPMSXL-5 magnetometer. Correction for the sample holder, as well as the diamagnetic correction χ_D, which was estimated from the Pascal constants,[10] was applied.

XSEED, POV-RAY, MESTRENOVA, and GOpenMol were used for the preparation of figures.[11]

CAUTION! *Perchlorate salts of metal complexes with organic ligands are potentially explosive.*[12] *The behavior of a few crystals of* **2**·CH$_3$CN *under physical stress was tested and did not show any sign of explosive decomposition, but proper precautions should be taken when handling these complexes.*

Details of the crystallographic measurements and crystallographic tables can be found in the Supporting Information.[13−17]

$[Fe_2(\mu\text{-}OH)(\mu\text{-}L_m)_2](ClO_4)_3$, 1. To the ligand L_m (0.190 g, 0.514 mmol) dissolved in methanol (10 mL) was added triethylamine (0.070 mL, 0.51 mmol). The Fe(ClO$_4$)$_2$·7H$_2$O (0.196 g, 0.514 mmol) was separately dissolved in methanol (5 mL), and the ligand/amine solution was added by cannula. A dark, air-sensitive green precipitate formed immediately. The reaction mixture was stirred for 3 h, after which time the system was filtered by cannula and dried under vacuum. The green precipitate was transported to the drybox and dissolved in methanol. Vapor diffusion tubes (methanol/Et$_2$O) set up in the drybox gave a green precipitate and a few colorless crystals after several days. Colorless crystals suitable for X-ray studies were mounted directly from the mother liquor as **1**·1.5CH$_3$OH. Anal. Calcd (Found) for C$_{40}$H$_{37}$Cl$_3$Fe$_2$N$_{16}$O$_{13}$: C, 41.14 (40.76); H, 3.19 (3.04); N, 19.19 (19.28). The green precipitate turns orange in open atmosphere and was not identified.

$[Co_2(\mu\text{-}OH)(\mu\text{-}L_m)_2](ClO_4)_3$, 2. To the ligand L_m (0.380 g, 1.03 mmol) dissolved in methanol (25 mL) was added triethylamine (0.143 mL, 1.03 mmol). The Co(ClO$_4$)$_2$·6H$_2$O (0.374 g, 1.03 mmol) was dissolved separately in methanol (6 mL), and the ligand/amine solution was added by cannula. A pink precipitate formed immediately. The reaction mixture was stirred for 5 h, after which time the system was filtered by cannula, washed with 5 mL of ether, and dried under vacuum overnight, affording 0.382 g (63%) of a pink solid. Single crystals suitable for X-ray studies were grown by vapor diffusion of Et$_2$O into 1 mL of acetonitrile solutions of the pink solid and were mounted directly from the mother liquor as **2**·CH$_3$CN. Anal. Calcd (Found) for C$_{40}$H$_{37}$Cl$_3$Co$_2$N$_{16}$O$_{13}$: C, 40.92 (40.72); H, 3.18 (3.07); N, 19.09 (19.22). MS ES(+) m/z (rel % abund) [assgn]: 1073 (1) $[Co_2(L_m)_2(OH)(ClO_4)_2]^+$, 898 (23) $[Co(L_m)_2(ClO_4)]^+$, 528 (53) $[Co_2(L_m)_2(ClO_4)_2]^{2+}$, 487 (19) $[Co_2(L_m)_2(OH)(ClO_4)]^{2+}$, 446 (10) $[CoL_mOH]^+$, 400 (90) $[Co(L_m)_2]^{2+}$, 292 (22) $[Co_2(L_m)_2(OH)]^{3+}$. HRMS ES$^+$ (m/z): $[Co_2(L_m)_2(OH)(ClO_4)]^{2+}$ calcd for $[C_{40}H_{37}Co_2N_{16}ClO_5]^{2+}$ 487.0737; found 487.0697. Preliminary X-ray diffraction studies indicated that the acetone solvate of the compound can be obtained by slow diffusion of Et$_2$O into the acetone solution of the pink solid.

$[Cu_2(\mu\text{-}OH)(\mu\text{-}L_m)_2](ClO_4)_3$, 3. This compound was prepared similarly to **2** starting from L_m (0.37 g, 1.0 mmol) dissolved in 12 mL of methanol and triethylamine (0.14 mL, 1.0 mmol) and Cu(ClO$_4$)$_2$·6H$_2$O (0.37 g, 1.0 mmol) dissolved in 4 mL of methanol. The resulting blue solid weighed 0.354 g (58%). A 40 mg sample of the blue solid was gently heated in a mixture of 6 mL of water and 3 mL of acetone until the solid completely dissolved. In 3−5 days at 5 °C blue crystals of **3**·2H$_2$O were isolated. Vapor diffusion of Et$_2$O into 1 mL of acetonitrile solutions of the blue solid results in crystals of **3**·1.5CH$_3$CN. Anal. Calcd (Found) for C$_{40}$H$_{37}$Cl$_3$Cu$_2$N$_{16}$O$_{13}$: C, 40.60 (40.84); H, 3.15 (3.05); N, 18.94 (19.03). MS ES(+) m/z (rel % abund) [assgn]: 1083 (22) $[Cu_2(L_m)_2(OH)(ClO_4)_2]^+$, 902 (40) $[Cu(L_m)_2(ClO_4)]^+$, 532 (48) $[Co_2(L_m)_2(ClO_4)_2]^{2+}$, 492 (40) $[Cu_2(L_m)_2(OH)(ClO_4)]^{2+}$, 450 (25) $[CuL_mOH]^+$, 433 (100) $[Cu(L_m)_2]^{2+}$, 371 (28) $[L_m + H]^+$, 294 (22) $[Cu_2(L_m)_2(OH)]^{3+}$. HRMS ES$^+$ (m/z): $[Cu_2(L_m)_2(OH)(ClO_4)_2]^+$ calcd for $[C_{40}H_{37}Cu_2N_{16}Cl_2O_9]^+$ 1081.0898; found 1081.0896.

$[Co_2(\mu\text{-}OH)(\mu\text{-}L_m^*)_2](ClO_4)_3$, 4. This compound was prepared similarly to **2** starting from L_m^* (0.25 g, 0.51 mmol) dissolved in 10 mL of methanol and triethylamine (0.070 mL, 0.51 mmol) and Co(ClO$_4$)$_2$·6H$_2$O (0.19 g, 0.51 mmol) dissolved in 4 mL of methanol. The resulting pink solid weighed 0.235 g (65%). Single crystals suitable for X-ray studies were grown by the vapor diffusion of Et$_2$O

into 1 mL of acetonitrile solutions of the pink solid and were mounted directly from the mother liquor as **4**. Anal. Calcd (Found) for $C_{56}H_{69}Cl_3Co_2O_{13}N_{16}$: C, 48.10 (48.21); H, 4.97 (4.98); N, 16.03 (16.08). MS ES(+) m/z (rel % abund) [assgn]: 1297 (32) $[Co_2(L_m*)_2(OH)(ClO_4)_2]^+$, 599 (100) $[Co_2(L_m*)_2(OH)(ClO_4)]^{2+}$, 416 (10) $[Co_2L_m*(ClO_4)_2]^{2+}$, 366 (80) $[Co_2(L_m*)_2(OH)]^{3+}$. HRMS ES$^+$ (m/z): $[Co_2(L_m*)_2(OH)(ClO_4)_2]^+$ calcd for $[C_{56}H_{69}Cl_2Co_2O_9N_{16}]^+$ 1297.3474; found 1297.3420.
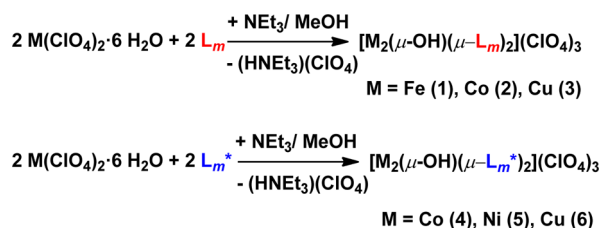
[Ni$_2$(μ-OH)(μ-L$_m$*)$_2$](ClO$_4$)$_3$, 5. This compound was prepared similarly to **2** starting from L_m* (0.25 g, 0.51 mmol) dissolved in 10 mL of methanol and triethylamine (0.070 mL, 0.51 mmol) and $Ni(ClO_4)_2 \cdot 6H_2O$ (0.19 g, 0.51 mmol) dissolved in 4 mL of methanol. The cloudy solution was cannula filtered, and the solvent was removed by rotary evaporation. The resulting green solid weighed 0.267 g (74%). Compound **5** was crystallized the same way as compound **2**. Anal. Calcd (Found) for $C_{56}H_{69}Cl_3Ni_2O_{13}N_{16}$: C, 48.11 (47.75); H, 4.97 (5.04); N, 16.03 (15.90). MS ES(+) m/z (rel % abund) [assgn]: 1297 (31) $[Ni_2(L_m*)_2(OH)(ClO_4)_2]^+$, 599 (100) $[Ni_2(L_m*)_2(OH)-(ClO_4)]^{2+}$, 511 (15) $[Ni(L_m*)_2]^{2+}$, 366 (95) $[Ni_2(L_m*)_2(OH)]^{3+}$. HRMS ES$^+$ (m/z): $[Ni_2(L_m*)_2(OH)(ClO_4)_2]^+$ calcd for $[C_{56}H_{69}Cl_2Ni_2O_9N_{16}]^+$ 1295.3517; found 1295.3478.

[Cu$_2$(μ-OH)(μ-L$_m$*)$_2$](ClO$_4$)$_3$, 6. This compound was prepared similarly to **2** starting from L_m* (0.25 g, 0.51 mmol) dissolved in 10 mL of methanol and triethylamine (0.070 mL, 0.51 mmol) and $Cu(ClO_4)_2 \cdot 6H_2O$ (0.19 g, 0.51 mmol) dissolved in 4 mL of methanol. The cloudy solution was cannula filtered, and the solvent was removed by rotary evaporation. The resulting green solid weighed 0.300 g (83%). Compound **6** was crystallized the same way as compound **2** and was taken directly from the mother liquor for the crystallographic studies as **6·2H$_2$O**. The 65 mg green precipitate remaining after the cannula filtration and crystallized in the same way as **6** also proved to be **6·2H$_2$O** by single-crystal X-ray diffraction. An analogous synthesis carried out in THF instead of methanol yields 0.342 g (95%) of a green precipitate. Single crystals grown with the same method proved to be **6·2H$_2$O**. Anal. Calcd (Found) for $C_{56}H_{69}Cl_3Cu_2O_{13}N_{16}$: C, 47.78 (47.79); H, 4.94 (5.03); N, 15.92 (15.84). MS ES(+) m/z (rel % abund) [assgn]: 1307 (5) $[Cu_2(L_m*)_2(OH)(ClO_4)_2]^+$, 604 (42) $[Cu_2(L_m*)_2(OH)(ClO_4)]^{2+}$, 562 (10) $[Cu(L_m*)_2(ClO_4)]^+$, 545 (100) $[Cu(L_m*)]^+$, 514 (5) $[Cu(L_m*)_2]^{2+}$, 483 (95) $[L_m* + H]^+$, 370 (80) $[Cu_2(L_m*)_2(OH)]^{3+}$.

■ RESULTS

Syntheses of the Metallacycles. The reactions of $M(ClO_4)_2 \cdot 6H_2O$ with the corresponding ligand L_m (M = Fe(II), Co(II), Cu(II)) or L_m* (M = Co(II), Ni(II), Cu(II)) in the presence of triethylamine resulted in the formation of the monohydroxide-bridged dinuclear metallacycles. The base was used to deprotonate the water molecules according to Scheme 2.

Scheme 2

2 $M(ClO_4)_2 \cdot 6 H_2O$ + 2 L_m $\xrightarrow[- (HNEt_3)(ClO_4)]{+ NEt_3/ MeOH}$ $[M_2(\mu\text{-}OH)(\mu\text{-}L_m)_2](ClO_4)_3$

M = Fe (1), Co (2), Cu (3)

2 $M(ClO_4)_2 \cdot 6 H_2O$ + 2 L_m* $\xrightarrow[- (HNEt_3)(ClO_4)]{+ NEt_3/ MeOH}$ $[M_2(\mu\text{-}OH)(\mu\text{-}L_m*)_2](ClO_4)_3$

M = Co (4), Ni (5), Cu (6)

Even in the presence of excess NEt$_3$, the monohydroxide-bridged compounds formed in all cases. Only a few colorless crystals of **1** were isolated; in the reaction the major product is a very air sensitive green powder that was not characterized. The synthesis of the hydroxide-bridged species, as opposed to oxide bridged analogues, is demonstrated by charge balance and

is corroborated by the characterization in solution of analogous zinc(II) and cadmium(II) compounds, where NMR resonances characteristic of the OH hydrogen were observed.[6c]

Mass Spectrometry. Positive-ion electrospray mass spectra (ESI$^+$-MS) of complexes **2–6** are similar. In all spectra, clusters such as $[M_2(L)_2OH(ClO_4)_2]^+$, $[M_2(L)_2OH(ClO_4)]^{2+}$, and $[M_2(L)_2OH]^{3+}$ corresponding to the complete hydroxide-bridged metallacycles are observed. Figure 1 shows the calculated and observed peaks for $[Co_2(\mu\text{-}OH)(\mu\text{-}L_m*)_2]$(ClO$_4$)$_3$, **4**, where the isotope patterns coupled with the high-resolution data definitively characterize these complexes. In the spectra of **2** and **3**, metallacycles formed with L_m, the $[M(L_m)_2]^{2+}$-type peaks have the highest intensities. For compounds **4–6**, the base peak is $[M_2(L_m*)_2OH(ClO_4)]^{2+}$ and the $[M_2(L_m*)_2OH]^{3+}$ species have very high intensities. The increase of the signal intensities for the metallacyclic species in the spectra of L_m* compounds, especially for $[M_2(L)_2OH]^{3+}$ (22% for **2**, **3** vs 80–95% for **4–6**), indicate that these metallacycles are more stable than the metallacycles formed with L_m under the conditions of these experiments.

Solid-State Structures. Figures 2–5 show the structures of the dinuclear hydroxide-bridged cations $[M_2(\mu\text{-}OH)(\mu\text{-}L)_2]^{3+}$, compounds **1–6**. The numbering scheme in Figure 4 is also correct for compound **1**, and similarly, Figure 5 is correct for **5** and **6·2H$_2$O**. Fully labeled figures are in the Supporting Information, Figures S1–S4. Selected bond distances and bond angles are shown in Table 1 and S2–S5.

In the structures of all compounds, except **3·2H$_2$O** and **3·1.5CH$_3$CN** (copper(II) complexes of L_m), the geometry around the metal centers is distorted trigonal bipyramidal, supported by the unusually large M–O–M angles (**1**: 156.4(4) Å, 161.7(17) Å; **2**: 166.8(2)°, 165.8(4)°) or perfectly linear M–O–M angles (**4–6**: 180°). Two pyrazolyl nitrogens and the hydroxide oxygen occupy the equatorial positions of the trigonal bipyramid, with N–M–N and N–M–O angles between 94.0° and 138.7°. In the axial positions the two remaining pyrazolyl nitrogens can be found enclosing N–M–N angles between 173.72° and 179.30°. The τ_5[19] values, summarized in Table 1, also indicate distorted trigonal bipyramidal geometry around the metal centers.

In the distorted trigonal bipyramidal structures of **1·1.5CH$_3$OH**, **2**, **4**, and **5** (complexes where the metal is not copper(II)), the axial and equatorial M–N bond distances are similar; for the first three the distances on average are 0.04 Å longer in the axial position, whereas for **5** they are 0.015 Å shorter. In contrast, in the copper(II) complex **6·2H$_2$O**, as expected because of the pseudo-Jahn–Teller effect, the structure is substantially axially compressed (Table S4): axial Cu–N 1.9875(18) Å, 1.9854(17) Å; equatorial Cu–N 2.2579(18) Å, 2.1218(18) Å.

The Cu–O–Cu angles in the two copper(II) metallacycles with L_m are significantly less than 180° (141.2° for **3·2H$_2$O**, 141.2° and 151.0° for **3·1.5CH$_3$CN**). This change in bridging angle results in two larger bond angles around the copper(II) centers (e.g., **3·2H$_2$O**: N(61)–Cu(1)–N(21) 175.81(8)° and O(1)–Cu(1)–N(51) 158.52(7)°), generating τ_5 values of 0.3 for **3·2H$_2$O** and 0.4 for **3·1.5CH$_3$CN**, typical of distorted square pyramidal geometry, especially for the former. This change is also reflected by the Cu–N bond lengths, with one longer axial, **3·2H$_2$O** Cu(1)–N(11) 2.2264(18) Å, and three shorter equatorial bond lengths, Cu(1)–N(21) 2.045(2) Å, Cu(1)–N(51) 2.0165(19) Å, and Cu(1)–N(61) 2.017(2) Å. The
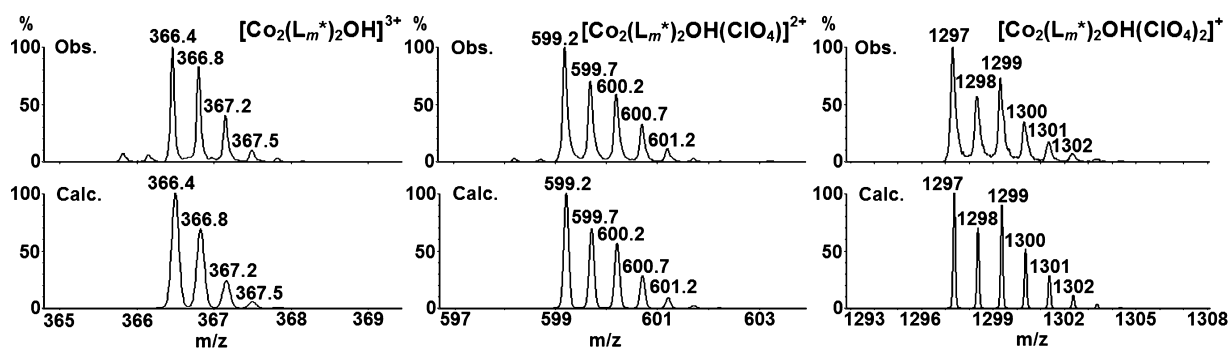
Figure 1. Observed (top) and calculated (bottom) ESI⁺-MS peaks corresponding to $[Co_2(L_m*)_2OH]^{3+}$, $[Co_2(L_m*)_2OH(ClO_4)]^{2+}$, and $[Co_2(L_m*)_2OH(ClO_4)_2]^+$ cationic units of $[Co_2(\mu\text{-}OH)(\mu\text{-}L_m*)_2](ClO_4)_3$, **4**.

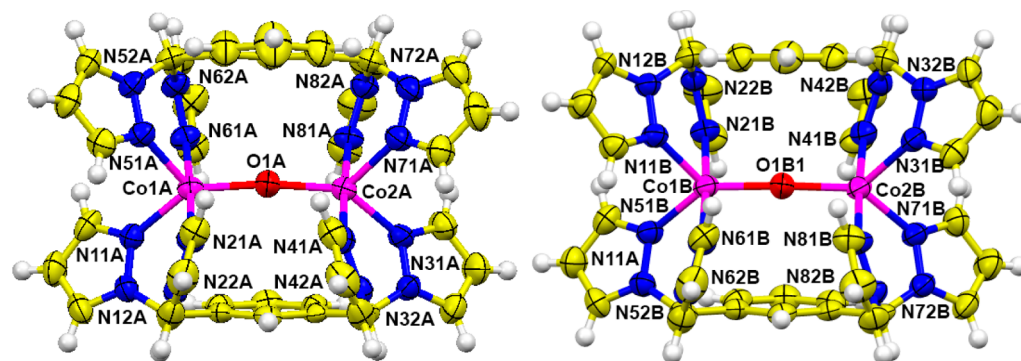**Figure 2.** Structure of the two independent $[Co_2(\mu\text{-}OH)(\mu\text{-}L_m)_2]^{3+}$ units of **2** at 295 K. Thermal ellipsoids are drawn at the 50% probability level. Disorder of O1A was removed for clarity of the figure.
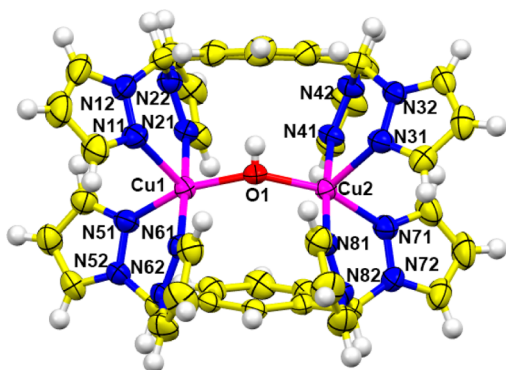

Figure 3. Structure of the $[Cu_2(\mu\text{-}OH)(\mu\text{-}L_m)_2]^{3+}$ unit of **3**·2H₂O at 100 K. Thermal ellipsoids are drawn at the 90% probability level.

oxygen from the bridging hydroxide group completes the equatorial plane.

The M−O distances for the L_m compounds are slightly shorter than predicted from the sum of the ionic radii,[18] while for the more sterically hindered L_m* metallacycles the M−O distances are longer than predicted (Table 1). This trend was previously noted in analogous fluoride-bridged complexes. In the data presented here, the only true direct comparison between the two ligands is with the cobalt(II) complexes, where the average Co−O distance in **2**·CH₃CN is 1.96 Å compared to the 2.0655(18) Å distance in the structure of the more sterically hindered **4** at the same temperature.

Compounds **4** and **5** undergo a phase change of order−disorder type at lower temperatures, but only the structure of **4** could be solved at 100 K (see crystallographic section for
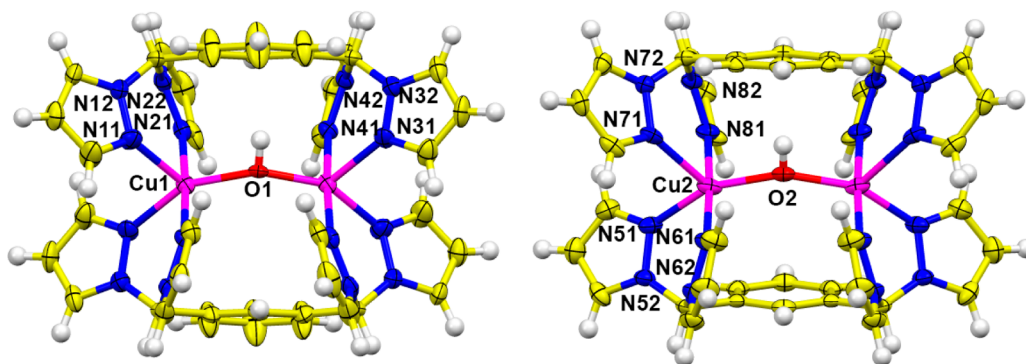

Figure 4. Structure of the two independent $[Cu_2(\mu\text{-}OH)(\mu\text{-}L_m)_2]^{3+}$ units of **3**·1.5CH₃CN at 150 K. Thermal ellipsoids are drawn at the 50% probability level. Disorder of O1 was removed for clarity of the figure.
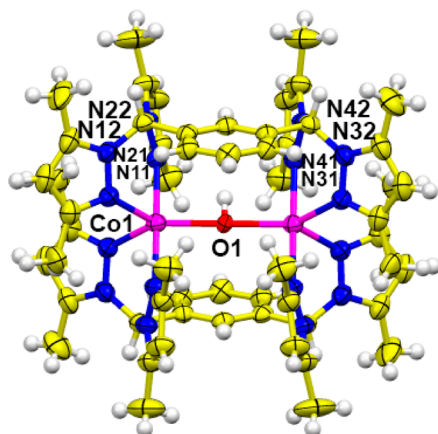
Figure 5. Structure of the $[Co_2(\mu\text{-OH})(\mu\text{-L}_m^*)_2]^{3+}$ unit of **4** at 295 K. Thermal ellipsoids are drawn at the 50% probability level. Disorder of the OH hydrogen was removed for clarity of the figure. At 100 K the inversion center is lost, Supporting Information, Figure S4.

details and Figure S5 in the Supporting Information). The phase change does not cause major structural changes that would significantly alter the properties of these compounds.

Magnetic Properties of the Copper(II) Complexes. The magnetic susceptibility data for the copper(II) complexes were interpreted using the standard Heisenberg–Dirac–Van Vleck Hamiltonian: $\hat{H} = -J\hat{S}_1\hat{S}_2$. In this notation, J is negative in the case of antiferromagnetic superexchange interactions. The magnetic susceptibility of a dinuclear copper(II) system is

$$\chi_d = \frac{N\mu_B^2 g^2}{3kT} \frac{6\exp(J/kT)}{1+3\exp(J/kT)} + 2TIP \quad (1)$$

As usually observed, the samples contained small amounts (less than 1%) of monomeric impurities. The monomer susceptibility can be calculated from:

$$\chi_m = (N\mu_B^2 g^2/3kT)\cdot 0.75 + TIP \quad (2)$$

At low temperatures these impurities dominated the magnetic susceptibility owing to very strong antiferromagnetic exchange interactions in the dinuclear species. For this reason, the monomeric contributions were removed from the experimental data (Figure 6) using

$$\chi_d = (\chi_{exp} - 2f\chi_m)/(1-f) \quad (3)$$

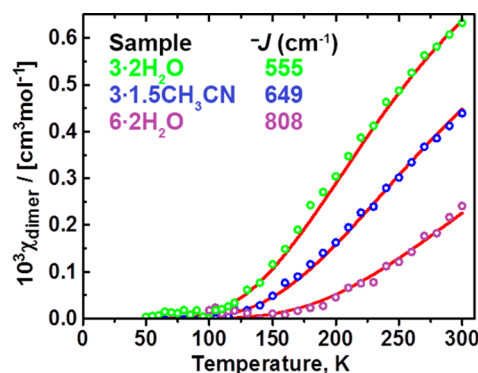**Figure 6.** Magnetic susceptibility of the copper(II) complexes. Green circles (top): $Cu_2(\mu\text{-OH})(\mu\text{-L}_m)_2](ClO_4)_3\cdot 2H_2O$ (**3·2H₂O**), blue circles (middle): $[Cu_2(\mu\text{-OH})(\mu\text{-L}_m)_2](ClO_4)_3\cdot 1.5CH_3CN$ (**3·1.5CH₃CN**), purple circles (bottom): $[Cu_2(\mu\text{-OH})(\mu\text{-L}_m^*)_2].(ClO_4)_3\cdot 2H_2O$ (**6·2H₂O**). Contribution from the monomeric impurities to the magnetic susceptibility was removed from the experimental data (see text). Circles are experimental data, solid lines calculated.

where f is the fraction of monomeric copper(II) species. The value for f was found from the low-temperature data, and subsequently the $-J$ values were extracted from the altered

Table 1. Structural Parameters for $[Fe_2(\mu\text{-OH})(\mu\text{-L}_m)_2](ClO_4)_3\cdot 1.5CH_3OH$ (1·1.5CH₃OH), $[Co_2(\mu\text{-OH})(\mu\text{-L}_m)_2](ClO_4)_3\cdot CH_3CN$ (2·CH₃CN), $[Cu_2(\mu\text{-OH})(\mu\text{-L}_m)_2](ClO_4)_3\cdot 2H_2O$ (3·2H₂O), $[Cu_2(\mu\text{-OH})(\mu\text{-L}_m)_2](ClO_4)_3\cdot 1.5CH_3CN$ (3·1.5CH₃CN), $[Co_2(\mu\text{-OH})(\mu\text{-L}_m^*)_2](ClO_4)_3$ (4), $[Ni_2(\mu\text{-OH})(\mu\text{-L}_m^*)_2](ClO_4)_3$ (5), and $[Cu_2(\mu\text{-OH})(\mu\text{-L}_m^*)_2](ClO_4)_3\cdot 2H_2O$ (6·2H₂O)

complex	temp, K	metal centers	M–O–M angle, deg	M–O distance, Å	predicted M–O distance, Å[b]	average M–N distance, Å	τ_5	M···M distance, Å
1·1.5CH₃OH	150	Fe(1)–Fe(1′)	156.4(4)	1.961[a]	2.03	2.136	0.59	3.839
		Fe(2)–Fe(2′)	161.7(17)	1.995(5)	2.03	2.152	0.61	3.939
2·CH₃CN	296	Co(1A)–Co(2A)	166.8(2)	1.969(3)/1.945(3)	1.99	2.108/2.103	0.71/0.72	3.888
		Co(1B)–Co(2B)	165.8(4)	1.962/1.983[a]	1.99	2.119/2.114	0.63/0.65	3.908
3·2H₂O	100	Cu(1)–Cu(2)	141.04(9)	1.9328(16)1.9413(16)	1.97	2.076/2.071	0.30	3.652
3·1.5CH₃CN	150	Cu(1)–Cu(1′)	141.2(3)	1.932[a]	1.97	2.112	0.42	3.644
		Cu(2)–Cu(2′)	151.0(2)	1.9653(11)	1.97	2.083	0.40	3.805
4	295	Co(1)–Co(1′)	180	2.0673(4)	1.99	2.118	0.74	4.135
4	100	Co(1)–Co(2)	177.61(10)	2.0655(18)2.0490(18)	1.99	2.109/2.107	0.73/0.72	4.114
5	295	Ni(1)–Ni(1′)	180	2.0640(10)	1.95	2.070	0.72	4.128
6·2H₂O	150	Cu(1)–Cu(1′)	180	2.0230(3)	1.97	2.088	0.68	4.046

[a]Average bond length, due to disorder. [b]Ref 18.
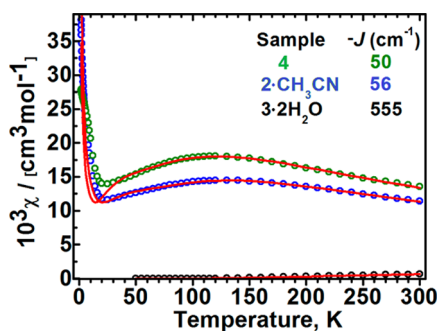
Figure 7. Magnetic susceptibility of $[Co_2(\mu\text{-}OH)(\mu\text{-}L_m)_2](ClO_4)_3\cdot$ CH_3CN ($2\cdot CH_3CN$), blue circles, and $[Co_2(\mu\text{-}OH)(\mu\text{-}L_m*)_2](ClO_4)_3$ (4), green circles (top). Circles are experimental data; solid lines, calculated. Data for $Cu_2(\mu\text{-}OH)(\mu\text{-}L_m)_2](ClO_4)_3\cdot 2H_2O$ ($3\cdot 2H_2O$) are also shown for comparison (plot at the bottom).

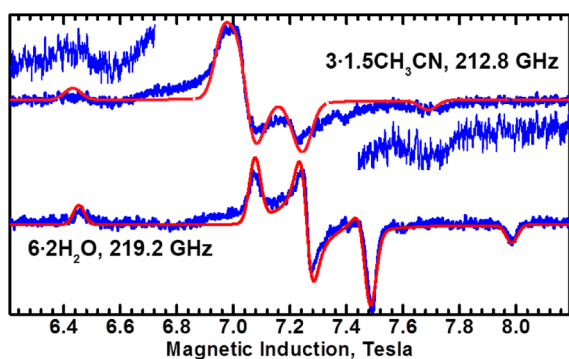**Figure 8.** High-frequency EPR spectra of the copper(II) complexes $3\cdot$ $1.5CH_3CN$ and $6\cdot 2H_2O$ recorded at 305 K with microwave frequencies as shown. The red lines are simulated with $g_x = 2.136$, $g_y = 2.035$, $g_z = 2.270$, $D = 0.280$ cm^{-1}, $E = 0.047$ cm^{-1} for $3\cdot$ $1.5CH_3CN$ and $g_x = 2.123$, $g_y = 2.310$, $g_z = 2.019$, $D = 0.235$ cm^{-1}, $E = 0.142$ cm^{-1} for $6\cdot 2H_2O$.
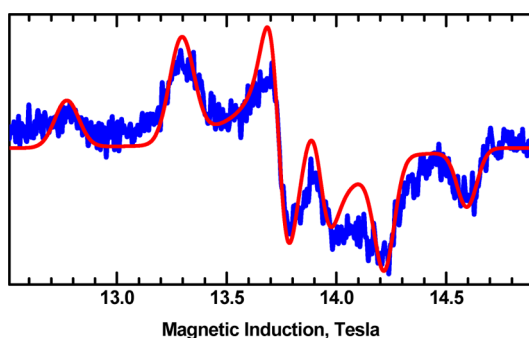

Figure 9. Blue: Spectrum of $3\cdot 2H_2O$ at 309 K, 412.8 GHz. Red: Simulation with $g_x = 2.130$, $g_y = 2.048$, $g_z = 2.263$, $D = 0.299$ cm^{-1}, $E = 0.028$ cm^{-1}.

experimental data above 100 K, as the dinuclear susceptibility is near zero at lower temperatures.

For the three $[Cu_2(\mu\text{-}OH)(\mu\text{-}L)_2](ClO_4)_3$ complexes, where $L = L_m$ or L_m*, χ_M decreases with the temperature, demonstrating strong antiferromagnetic superexchange interactions between the copper(II) centers. The magnetic moment (per one copper(II)) at 300 K is 0.98 μ_B for $3\cdot 2H_2O$, 0.75 μ_B for $3\cdot 1.5CH_3CN$, and 0.68 μ_B for $6\cdot 2H_2O$, very small compared to the magnetic moment for a noninteracting copper(II) center (ca. 1.82 μ_B). The antiferromagnetic exchange coupling

constant, $-J$, is 555 cm^{-1} for $3\cdot 2H_2O$, 649 cm^{-1} for $3\cdot$ $1.5CH_3CN$, and 808 cm^{-1} for $6\cdot 2H_2O$.

Single-crystal X-ray diffraction data showed that there are two crystallographically independent $[Cu_2(\mu\text{-}OH)(\mu\text{-}L_m)_2]^{3+}$ cations in the unit cell of $3\cdot 1.5CH_3CN$, with Cu−O−Cu angles of 141.2° and 151.0°, respectively. The $-J$ value of 649 cm^{-1} obtained from the magnetic data fitting represents an average of the two species.

Magnetic Properties of the Cobalt(II) Complexes. Zero-field splitting (zfs) exists on separate multielectron ions such as cobalt(II), and it affects the magnetic properties of the dinuclear complexes. To account for zfs, the magnetic data for the cobalt(II) systems were interpreted using the Hamiltonian

$$\hat{H} = -J\hat{S}_1\hat{S}_2 + D\{\hat{S}_{z1}^2 - S_1(S_1 + 1)/3\} + E(\hat{S}_{x1}^2 - \hat{S}_{y1}^2)$$
$$+ D\{\hat{S}_{z2}^2 - S_2(S_2 + 1)/3\} + E(\hat{S}_{x2}^2 - \hat{S}_{y2}^2)$$
$$+ \mu_B B\{\mathbf{g}_1\}\hat{S}_1 + \mu_B B\{\mathbf{g}_2\}\hat{S}_2 \tag{4}$$

The spin Hamiltonian matrix was diagonalized to find the energy levels, and the magnetic susceptibility per mole of dimer was calculated from

$$\chi_d = -\frac{N}{B}\frac{\sum_i \frac{\partial E_i}{\partial B}\exp(-E_i/kT)}{\sum_i \exp(-E_i/kT)} \tag{5}$$

The derivatives $\delta E_i/\delta B$ were evaluated numerically by calculating the energy levels slightly below and slightly above (± 5 G) the operational magnetic field of a SQUID magnetometer (5000 G).

As clearly indicated in Figure 7, which includes data for one of the copper(II) complexes, and Table 2, the antiferromag-

Table 2. Spin Hamiltonian Parameters for the $[Co_2(\mu\text{-}OH)(\mu\text{-}L)_2](ClO_4)_3$ Complexes, Where $L = L_m$ (2) or L_m* (4)

complex	$-J$ (cm^{-1})	D (cm^{-1})	g_{av}
$2\cdot CH_3CN$	56	−30	2.33
	51	67	2.29
4	50	−30	2.47
	48	47	2.45

netic interactions for the cobalt(II) complexes are weaker than for the copper(II) compounds, but still substantial. Relatively high contents of monomeric impurities, 2% in $2\cdot CH_3CN$ and 1.4% in 4, were observed, impacting the quality of the low-temperature susceptibility data. The monomeric cobalt(II) impurities are likely to have large zero-field splitting, complicating the low-temperature magnetic behavior; attempts of taking that kind of zfs into account were not successful. Higher temperature data, above ~30 K, were sufficient to determine the $-J$ values in these dinuclear species. Contrary to what has been observed in our recent paper on analogous fluoride-bridged compounds of the type $[Co_2(\mu\text{-}F)(\mu\text{-}L_m*)_2]^{3+}$,[6a] the sign of the D parameters could not be determined from the magnetic data, and in Table 2 we report fitting results with both positive and negative D. The effect of the sign of D on the $-J$ value is moderate. The magnitude of D is not surprising, as high-spin cobalt(II) in other complexes was found to exhibit even larger zero-field splitting.[20]

The data for the nickel(II) complex were not interpretable, presumably due to the high contents of monomeric impurities

Table 3. Spin Hamiltonian Parameters for the $[Cu_2(\mu\text{-OH})(\mu\text{-L})_2](ClO_4)_3$ Complexes, Where L = L_m (3) or L_m^* (6)

complex	$-J$ (cm^{-1})	g_x	g_y	g_z	$|D|$ (cm^{-1})	$|E|$ (cm^{-1})
3·1.5CH$_3$CN	649(1)	2.14[a]	2.03[a]	2.27[a]	0.28	0.047
3·2H$_2$O	555(3)	2.130[a]	2.048[a]	2.263[a]	0.299	0.028
		2.083[b]	2.048[b]	2.310[b]		
		2.130[c]	2.263[c]	2.048[c]	0.191[c]	0.136[c]
6·2H$_2$O	808(50)	2.123[d]	2.310[d]	2.019[d]	0.235	0.142

[a]Coupled-spin state g values. [b]Single-ion g values (see Figure 10 and the text). [c]An equivalent parameter set (see text and SI) allowing a direct comparison to the parameters of 6·2H$_2$O. [d]The coupled-spin and the single-ion g values are equal in a centrosymmetric dinuclear system. Note: The errors in $-J$ (in parentheses) were calculated by the fitting software. However, there are experimental uncertainties, such as the Pascal corrections, errors in the molar mass, etc., which may significantly affect the fitting results. The errors in such magnetic fittings of $-J$ are often estimated to be on the order of 5−10%.

with large zfs. The small sample size available for $[Fe_2(\mu\text{-OH})(\mu\text{-}L_m)_2](ClO_4)_3 \cdot 1.5CH_3OH$ prevented collection of magnetic data.

EPR. Only the copper(II) complexes showed EPR spectra (Figures 8 and 9), while the cobalt(II) and nickel(II) analogues were EPR-silent at any frequency and temperature. In a coupled cobalt(II) system, the D parameter on a single ion (eq 4) of −30 cm^{-1} (Table 2) contributes +72 cm^{-1} to the D parameter of the coupled triplet state (eq 6),[21] far above the possibilities of our high-field EPR instrument, where the maximum microwave quantum energy is about 14 cm^{-1}. This effect is not so strong in the case of nickel(II) dinuclear systems, but all complexes studied here exhibited strong nonresonant microwave absorption affecting even the quality of the spectra of the copper(II) complexes. Spectra of the copper(II) compounds were very weak and noisy even at 309 K, yet well reproducible, but could not be recorded at low temperatures as a result of the strong antiferromagnetic interactions. A standard spin Hamiltonian for $S = 1$ was used to interpret these spectra:

$$\hat{H}_S = \mu_B \mathbf{B} \cdot \{\mathbf{g}\} \cdot \hat{\mathbf{S}} + D\{\hat{S}_z^2 - S(S+1)/3\} + E(\hat{S}_x^2 - \hat{S}_y^2) \quad (6)$$

The presence of two different species in 3·1.5CH$_3$CN causes very broad and ill-defined resonances in its spectrum, and the parameters above represent an average of the two species. Sample 6·2H$_2$O produced spectra of much better quality than 3·2H$_2$O and 3·1.5CH$_3$CN in the 200 GHz frequency range, but no spectrum could be recorded in the 400 GHz range. Opposite of this, the best spectrum of 3·2H$_2$O was obtained with 412.8 GHz at 309 K, the highest temperature possible in our experimental setup. While very weak and noisy, this spectrum (Figure 9) is very well reproducible.

The signs of the D and E parameters could not be determined, and the absolute values are listed in Table 3. However, E must have the same sign as D in each case. An interesting feature of the complex 6·2H$_2$O is the low value, 2.02, of one of its g components. Analogous complexes such as $[Cu_2(\mu\text{-F})(\mu\text{-L})_2](BF_4)_3$, L = L_m or L_m^*, have one of the g components exactly 2, indicating that the ground-state orbital of copper(II) is d_{z^2} instead of $d_{x^2-y^2}$, the orbital more commonly encountered among copper(II) complexes. This appears to be not fully realized in 6·2H$_2$O. DFT calculations (vide infra) indicate that the ground state in our OH$^-$-bridged species is a mixture of d_{z^2} and $d_{x^2-y^2}$. The $d_{x^2-y^2}$ character is most pronounced in 3·2H$_2$O, while the d_{z^2} character is prevalent in 6·2H$_2$O. Another characteristic feature is the very strong "rhombicity" of the EPR parameters: three very different g values and E parameter comparable to D. The mixed character of the ground state, particularly in 6·2H$_2$O, introduces an

ambiguity in assigning the g values: it must be decided which of the g components will be labeled "z". In a pure d_{z^2} case, the smallest g should be named g_z, and also it should be closer to 2 than that found in 6·2H$_2$O (2.019). In 3·2H$_2$O there is less ambiguity because the smallest g component is significantly larger than that in 6·2H$_2$O and calls for the $d_{x^2-y^2}$-type parameters. When choosing $g_z = 2.019$, one obtains the parameter set for 6·2H$_2$O: $g_x = 2.123$, $g_y = 2.310$, $g_z = 2.019$, $D = 0.235$ cm^{-1}, $E = 0.142$ cm^{-1} (Figure 8). A choice of the 2.310 component as g_z results in a parameter set $g_x = 2.123$, $g_y = 2.019$, $g_z = 2.310$, $D = 0.330$ cm^{-1}, $E = 0.046$ cm^{-1}. These two sets are equivalent and result in the same EPR simulation. By convention, one would be tempted to choose the latter parameter set with $|E| < |D/3|$, but the former one is useful in discussing the zero-field splitting parameters in 6·2H$_2$O and even more so in similar linear M−X−M bridged complexes.[6]

For 3·2H$_2$O we found $g_x = 2.130$, $g_y = 2.048$, $g_z = 2.263$, $D = 0.299$ cm^{-1}, $E = 0.028$ cm^{-1}. The g parameters for 3·2H$_2$O and 6·2H$_2$O are not fully comparable because of the way the g matrices of two interacting ions combine to give the coupled-spin state g. Complex 6·2H$_2$O has an inversion center and the corresponding g components of two ions are parallel; that is, g_{x1} is parallel to g_{x2}, etc. As a result, the g matrix in the triplet spin state has the same values and axes as the g matrices of the two ions. On the other hand, 3·2H$_2$O does not possess an inversion center and the principal directions of the g matrices of two ions are not parallel. It would be easy to find the triplet-state g matrix if the individual g matrices were known. But here, we know the coupled g matrix and have to extract the individual ones. DFT calculations of the g matrix on each copper(II) ion were performed using the ORCA package (see below). The directions of g components on each copper(II) ion were found (Figure 10), which were in agreement with the expectations. The direction of the smallest g component was within 6° from the Cu−N$_{axial}$ vectors (vertical bonds in Figure 10). The direction of the largest g was 13.2° from the longest Cu−N bond on one copper and 8.3° on another. The directions of the intermediate g deviate from the respective Cu−O vectors on two ions by 8.8° and 7.3°. Next, the g component values, assumed to be equal on both ions, were chosen by trial and error. The g matrix of Cu(2) (G_2 in matrix notation) was rotated into the axes of Cu(1), and the result was added to the g matrix of Cu(1) to obtain the nondiagonal triplet state G_T matrix. In matrix notation, $G_T = (A^T G_2 A + G_1)/2$, where A is the transformation matrix from the axes of G_2 to G_1. G_T was subsequently diagonalized to evaluate its main values and axes. This process was repeated until the resulting G_T main values were equal to the triplet state g components found from EPR. This task could have been infeasible, but was facilitated by the
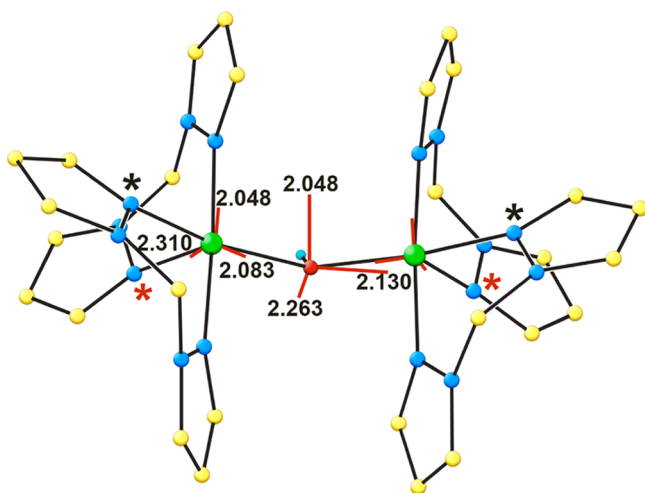
Figure 10. Principal directions of the local *g* matrices of two copper(II) ions in **3**·2H$_2$O compared to those of the triplet state *g* matrix. The local *g* components are assumed equal on the two ions, and their directions are indicated by the red lines. The directions of the coupled *g* matrix are along the red lines centered on the bridging oxygen. The light blue dot is the OH$^-$ hydrogen atom. The nitrogen atoms marked with * and the bridging O all lie almost exactly in one plane, from which the two copper(II) atoms deviate by only 0.032 and 0.004 Å. The directions of the single-ion *g* = 2.048 components are almost perpendicular to that plane at −84° and 86°, while in the triplet state the corresponding angle is 88°. Red asterisks mark the N atoms with the longest Cu−N bonds. A similar diagram for **6**·2H$_2$O is shown in Figure S7 in the Supporting Information.

fact that the directions of the smallest *g* components on two copper(II) atoms were almost parallel, with just an angle of 7.2° between them. The single-ion *g* values obtained from this procedure, $g_x = 2.048$, $g_y = 2.083$, $g_z = 2.310$, are consistent with the predominantly $d_{x^2-y^2}$ ground state.

"Broken Symmetry" DFT Calculation of the Exchange Integrals (−*J*). "Broken symmetry" density functional theory calculations were performed by using the software ORCA[22] to estimate and rationalize the magnitude of the exchange integral. A self-consistent field (SCF) calculation is first performed for the maximum spin state of the dinuclear species. Next, a "broken symmetry" state is set up with all unpaired electrons being spin-up on one metal and spin-down on the other, and another SCF calculation is run. The energies of the high-spin and broken symmetry states are finally used to estimate the exchange integral value, −*J* (for Hamiltonian $\hat{H} = -J\hat{S}_1\hat{S}_2$) based on the equation $-J = 2(E_{HS}-E_{BS})/(\langle S^2\rangle_{HS} - \langle S^2\rangle_{BS})$, where E_{HS} and E_{BS} are the energies of the high-spin (HS) and the broken-symmetry (BS) states and $\langle S\rangle^2$ are the expectation values of the spin-squared operator in the HS and BS states. Ahlrichs-type basis set TZVPP for copper(II) and SVP for other atoms were used, combined with the B3LYP functional.[23] Ahlrichs polarization functions from basis H - Kr R and auxiliary bases from the TurboMole library were also used.[24]

The molecules were simplified by removing the methyl groups on the pyrazolyl fragments as well as the benzene rings and placing hydrogen atoms at appropriate locations. All remaining atoms were retained at the positions determined by the X-ray structures. The coordinate system for the complexes with d_{z^2} ground state, representing all but one case (**3**·2H$_2$O), was chosen with the X axis along the metal−O vector and the Z axis perpendicular to the plane of oxygen and two equatorial nitrogen atoms. For **3**·2H$_2$O, with $d_{x^2-y^2}$ ground state, the Z axis

was normal (or perpendicular) to the least-squares plane of the bridging O atom and the three short-distance N atoms. The Y axis was perpendicular to both Z and Cu−O.

Table 4 shows the results of these calculations for the copper(II) compounds. Although the Cu−O−Cu angle in **3**·

Table 4. Spin Densities and Orbital Interactions for the Copper(II) Complexes As Calculated from the "Broken Symmetry" DFT Method

	3·2H$_2$O[a]	3·1.5CH$_3$CN[b]	3·1.5CH$_3$CN[b]	6·2H$_2$O[b]
Cu−O−Cu (deg)	141.0	141.2	151.2	180
Spin Density				
Cu[c]	0.658	0.665	0.664	0.667
O	0.153	0.157	0.144	0.136
N on trigonal axis	0.094	0.098	0.095	0.102
	0.085	0.089	0.089	0.084
N in trigonal plane	0.074	0.051	0.065	0.049
	0.005	0.016	0.010	0.024
overlap integral	0.172	0.156	0.191	0.203
$E_{antisym} - E_{sym}$ (cm^{-1})[d]	5710	5280	6430	6730
Exchange Integral −*J*, cm^{-1}				
calcd, DFT	700	514	916	994
exptl	555	649		808

[a]The system of coordinates was chosen with the Z axis along the tetragonal pyramid axis and X axis close to Cu−O. [b]The system of coordinates was chosen with the Z axis along the trigonal bipyramid axis and X axis close to Cu−O. [c]Average of two copper(II) ions. [d]Calculated from the averages of the spin-up and spin-down energies of the respective antisymmetric and symmetric orbitals.

2H$_2$O (141.0°) is the same as in one of the species in **3**·1.5CH$_3$CN (141.2°), the −*J* value calculated from DFT for the latter is much smaller than the one calculated for the former. This difference appears to be associated with the character of the ground state, which is more of the $d_{x^2-y^2}$ type in **3**·2H$_2$O than in **3**·1.5CH$_3$CN, allowing for a stronger overlap of the magnetic orbitals. The ground-state character is reflected in the spin densities on the axial and equatorial nitrogen ligands (Figure 11 and Table 4).

The ratio of −*J* calculated from DFT, Table 4, to the experimental −*J* in **3**·2H$_2$O and in **6**·2H$_2$O is 1.26 and 1.23, respectively; therefore we took a ~1.24 factor as the systematic overestimation error in these DFT calculations. The corrected DFT values of −*J* for the two molecules in **3**·1.5CH$_3$CN would then be −415 cm^{-1} for the molecule with the 141.2° Cu−O−Cu angle and −739 cm^{-1} for that with the 151.2° Cu−O−Cu angle. The average of these two numbers, 577 cm^{-1}, compares reasonably with the experimental −*J* value, 649 cm^{-1} for **3**·1.5CH$_3$CN.

As shown in Table 5, the calculations match the measured weaker, but still substantial, antiferromagnetic interactions for the cobalt(II) complexes. Similar trends were observed previously for the fluoride-bridged analogues.

The DFT calculation of the single-ion *g* components was performed on the dinuclear molecules of **3**·2H$_2$O and of **6**·2H$_2$O, simplified in the same manner as described above. In calculations for Cu(1), Cu(2) was replaced by Zn and vice versa. The magnitudes of $\Delta g_i = g_i − 2.0023$, where $i = x, y, z$, were seriously underestimated by the calculation. Three very different *g* values were produced, in agreement with the experiment. The main aim of these calculations was finding the directions of the *g* components rather than their magnitudes.
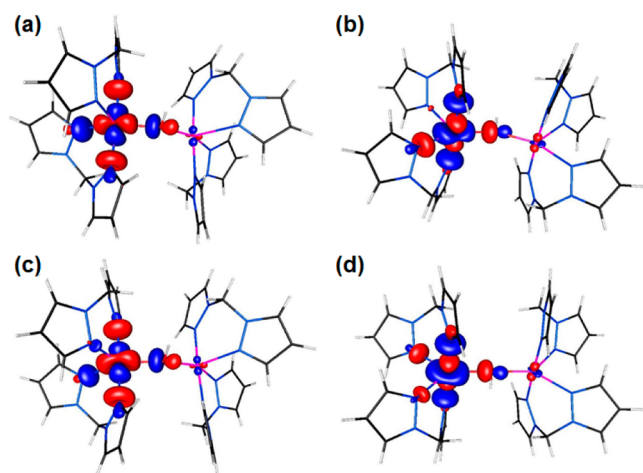
Figure 11. Change of the ground-state character from predominatly $d_{x2−y2}$ character to predominatly d_{z2} character: **3**·2H$_2$O (a), **3**·1.5CH$_3$CN, Cu−O−Cu 151° (b), **3**·1.5CH$_3$CN Cu−O−Cu 141° (c), and **6**·2H$_2$O (d). The participation in the magnetic orbital of one of the equatorial nitrogen ligands (using the trigonal bipyramid nomenclature) is increasing from (a) to (d) and correlates with the τ_5 values (0.30, 0.42, 0.40, and 0.68 respectively), indicating increasing d$_{z^2}$ character.

Table 5. Spin Densities and Overlap Integrals of the Three Magnetic Orbitals for the Cobalt(II) Complexes As Calculated from the "Broken Symmetry" DFT

	4	2·CH$_3$CN
M−O−M (deg)	180	166.8
Spin Density		
M	2.767	2.748
O	0.098	0.119
N on trigonal axis	0.034	0.034
	0.039	0.040
N in trigonal plane	0.034	0.035
	0.034	0.032
overlap integral	0.111	0.139
	0.066	0.083
	0.001	0.006
Exchange Integral −J, cm^{-1}		
calcd, DFT	58	99
exptl[a]	50, 48	56, 51

[a]determined with negative and positive D, respectively, see Table 2.

■ DISCUSSION

We have synthesized two series of [M$_2$(μ-OH)(μ-L)$_2$](ClO$_4$)$_3$ complexes with **L$_m$** and **L$_m$***, by deprotonation of the water of crystallization of the starting perchlorate salts, in order to probe the effects of changing the metal centers and bridging ligands on the geometry and magnetic properties of the metallacycles. Previous work by others has demonstrated that the geometry of the metal coordination environment and the position and type of bridging groups greatly affect the magnetic interactions between the metal centers,[7] but the complexes reported here represent the first extensive series of monohydroxide-bridged compounds where the M−O−M angle is large or in some cases exactly 180°.

The M−O−M angle is the main metric that defines the geometry around the metal centers: distorted trigonal bipyramidal for large or linear angles (156−180°) or more toward distorted square pyramidal for bent M−O−M angles (141−151°). As previously demonstrated with analogous [M$_2$(μ-F)(μ-L)$_2$]$^{3+}$ complexes, these ditopic (pyrazolyl)methane ligands form dinuclear complexes that favor the trigonal bipyramidal geometry over the generally more common square pyramidal,[25] especially the more bulky **L$_m$*** ligand. The copper(II) compounds with both ligands undergo pseudo-Jahn−Teller distortions that cause the expected bond length anomalies (axially elongated square pyramid for **3**·2H$_2$O and axially compressed trigonal bipyramid for **6**·2H$_2$O).[26]

For compounds **4**−**6**, the M−O−M angle is exactly 180°. These and previous results suggest that the metallacycles of the bulkier **L$_m$*** ligand favor a structure where the M−O−M angle is 180°. While a large number of hydroxide-bridged compounds have been synthesized,[27] we were unable to find any examples of a perfectly linear M−O(H)−M bridge and only a couple of examples of nearly linear hydroxide bridges.[28,29] Some of these bridges are supported by sterically protecting, large porphyrin ligands. The Fe−O−Fe angle of 173.6°, close to perfect linearity, was measured for [(tpp)Fe−O(H)−Fe-(tpp)]-(CB$_{11}$H$_6$Cl$_6$)·toluene (tpp = tetraphenylporphyrinate).[28a] Another example of a monohydroxide-bridged compound [Cu$_2$(L^{21})(OH)](CF$_3$SO$_3$)$_3$·H$_2$O, L^{21} = amino-cryptand, with an M−O−M angle close to 180° was reported by the Nelson group where the hydroxide bridge is supported by amino-cryptands; the Cu−O−Cu is 174.0°.[29]

Hoffmann and co-workers[7b] worked with theoretical models investigating the relationship between structure and magnetism of a model five-coordinate copper(II) compound [Cl$_4$CuClCuCl$_4$]$^{5-}$ in both trigonal bipyramidal and square pyramidal geometry. The results showed that in the trigonal bipyramidal geometry the unpaired electron of each copper(II) is located in a d$_{z^2}$-shaped orbital. The singlet−triplet energy gap, which corresponds to the intramolecular exchange coupling constant, −J, involves the sideways symmetric antibonding combination of the copper(II) 3d$_{z^2}$-shaped orbitals with the Cl s orbital and the sideways antisymmetric combination of the same metal orbitals with a Cl 3p$_x$ orbital. Consequently the −J values are excellent descriptors of the strength of the antiferromagnetic exchange interactions. Upon distortion of the trigonal bipyramidal geometry into square pyramidal, the highest energy orbital becomes a d$_{x^2−y^2}$-type orbital (basal plane of the square pyramid), and the bridging ligand becomes axial. The bridging ligand has no orbitals with the proper symmetry to interact with the d$_{x^2−y^2}$-type orbitals. The symmetric and antisymmetric combinations of the two orbitals remain degenerate in such a dinuclear compound, and there is no expected magnetic interaction of the unpaired electrons. As the geometry is distorted from square pyramidal to trigonal bipyramidal, the degeneracy of these states is lifted, allowing better interactions between the metal centers and increasing the singlet−triplet energy gap.

Although the change in the Cu−O−Cu angle of the [Cu$_2$(μ-OH)(μ-L)$_2$](ClO$_4$)$_3$, L = **L$_m$** or **L$_m$***, compounds from 180° for **6**·2H$_2$O to 151.0−141.0° in **3**·2H$_2$O and **3**·1.5CH$_3$CN results in the distortion of the geometry around copper(II) from a geometry resembling a trigonal bipyramid into one more square pyramidal, in contrast to the similar distortion presented by Hoffmann,[7b] in **3**·2H$_2$O the hydroxide remains in the equatorial position of the distorted square pyramid. Therefore, significant antiferromagnetic superexchange interactions are still promoted through the d$_{x^2−y^2}$ and the oxygen s and p$_x$ orbitals. The axial site is occupied by one of the four nitrogen atoms of **L$_m$**. The "broken-symmetry" DFT calculations for **3**·2H$_2$O and **3**·

1.5CH$_3$CN show increasing participation of one of the equatorial nitrogen ligands (using the trigonal bipyramidal nomenclature) in the magnetic orbital of copper(II) in the sequence **3**·2H$_2$O < **3**·1.5CH$_3$CN (151°) < **3**·1.5CH$_3$CN (141°) < **6**·2H$_2$O, which may be used as a measure of the increasing d$_{z^2}$ character of the magnetic orbital (Table 4, Figure 11). This geometrical distortion from a geometry with more square pyramidal character than trigonal bipyramidal is also reflected by the τ_5 values:[19] 0.30 for **3**·2H$_2$O (141°) < 0.40 for **3**·1.5CH$_3$CN (151°) < 0.42 for **3**·1.5CH$_3$CN (141°) < 0.68 for **6**·2H$_2$O (180°).

While the Cu···Cu nonbonding distance in **6**·2H$_2$O is 0.2–0.4 Å longer than in the analogous **3**·2H$_2$O and **3**·1.5CH$_3$CN, the Cu–O–Cu angle is larger by approximately 30–40°, resulting in a Cu–O–Cu angle of 180°. This unique linear arrangement promotes unusually strong antiferromagnetic superexchange interactions, with −J = 808 cm^{-1}. The "broken-symmetry" DFT calculations showed that the exchange integral is larger than the ones previously reported[6] for [Cu$_2$(μ-X)(μ-L$_m$*)$_2$](BF$_4$)$_3$ (X = F$^-$, Cl$^-$), and it is close to the Br$^-$-bridged analogue, where the Cu–X–Cu angle is fixed at 180° (0.125, 0.187, 0.228, respectively, vs 0.203 for **6**·2H$_2$O in the triplet state). The spin delocalization toward the bridging oxygen s (0, 0.0053, 0.0055, respectively vs 0.0061) and p$_x$ (0.072, 0.096, 0.116, respectively, vs 0.123) orbitals is larger than any of the halide-bridged compounds, probably also a result of the unusual linearity of the Cu–O–Cu angle.

In this work the magnetic data for copper(II) could be compared only with the magnetic properties of analogous cobalt(II) complexes. The lower −J, ca. 50 cm^{-1}, for the cobalt(II) hydroxide complexes **2**·CH$_3$CN and **4** versus the copper(II) hydroxide complexes was supported by the DFT calculations and was expected given that −J values decrease with the square of the number of unpaired electrons on the metal.[7b] The −J values for copper(II) and cobalt(II) complexes observed here, as well as in ref 6a, roughly obey this rule. We note that for both [Cu$_2$(μ-OH)(μ-L$_m$*)$_2$]$^{3+}$/[Cu$_2$(μ-F)(μ-L$_m$*)$_2$]$^{3+}$ and [Co$_2$(μ-OH)(μ-L$_m$*)$_2$]$^{3+}$/[Co$_2$(μ-F)(μ-L$_m$*)$_2$]$^{3+}$ pairs, the ratio of the −J values is similar, about 1.5, showing that both the copper(II) and the cobalt(II) hydroxide complexes have stronger antiferromagnetic interactions than the analogous fluoride-bridged complexes.

Five-coordinate, dinuclear copper(II) compounds with a single hydroxide bridge connecting the metal centers, for which both structural and magnetic data are available, are shown in Table 6. These complexes are listed in order of increasing −J and show the general trends described above; however Table 6 contains exceptions to the trends for which there are currently no explanations.

In the two recent studies that summarize the magneto-structural correlations in monohydroxide-bridged copper(II) complexes,[30,31] it was argued that the main structural feature affecting the geometry and thus the magnitude of the intramolecular exchange coupling constant (−J) is the Cu–O–Cu angle. As a consequence of larger Cu–O–Cu angles, the Cu···Cu nonbonding distance becomes longer than in analogous compounds with bent Cu–O–Cu angles by 0.2–0.4 Å. The change in the Cu···Cu separation does not affect the antiferromagnetic interactions as drastically as the changes in the Cu–O–Cu angle.

The compound [Cu$_2$(L^{21})(OH)](CF$_3$SO$_3$)$_3$·H$_2$O, L^{21} = amino-cryptand, (Table 6) with a Cu–O–Cu angle of 174.0°, synthesized by Nelson et al.,[29] exhibits strong antiferromagnetic behavior, with −J = 865 cm^{-1}. The geometry around the metal centers is trigonal bipyramidal, and the Jahn–Teller axes are pointing at each other. This arrangement allows the most advantageous overlap of the copper(II) d$_{z^2}$ and the oxygen p$_z$ orbitals and explains the efficient antiferromagnetic superexchange. On the contrary, in **6**·2H$_2$O while the geometry is also trigonal bipyramidal, the Jahn–Teller axes are perpendicular to the Cu···Cu direction. Interestingly, this arrangement, where the d$_{z^2}$ orbital is overlapping the bridging group with the "doughnut" portion, still results in unexpectedly high exchange coupling constants, −J = 808 cm^{-1}, comparable with −J for Nelson's compound.

The −J values for the copper(II) compounds where the monohydroxide bridge is in the equatorial plane of the trigonal bipyramid, similarly to **6**·2H$_2$O, vary between 86 and 322 cm^{-1}. The larger energy gap, −J = 322 cm^{-1}, measured for [Cu$_2$(L^7)$_4$(OH)](ClO$_4$)$_3$ (L^7 = 2,2'-bipyridine)[37] is a very special case where one copper(II) center is trigonal bipyramidal with the hydroxide in the equatorial position, but the other copper(II) is in a square pyramidal geometry. This unusual arrangement cannot be compared directly to **6**·2H$_2$O. The only monohydroxide-bridged compound with the exact same geometry as **6**·2H$_2$O is [Cu$_2$(L^1)(OH)](ClO$_4$)$_3$·2H$_2$O (L^1 = 1,4,8,11-tetrakis(2-pyridylmethyl)-1,4,8,11-tetraazacyclotetradecane),[32] with a Cu–O–Cu angle 134.6°. This compound is weakly antiferromagnetic, −J = 86 cm^{-1}; the singlet–triplet energy gap is 10 times smaller than the one measured for **6**·2H$_2$O, −J = 808 cm^{-1}. These results support our original statement above, that the strength of the antiferromagnetic interaction for **6**·2H$_2$O must be a consequence of the unusual linearity of the Cu–O–Cu angle, 180°, which provides the most efficient superexchange pathway for this type of geometry. The other two new copper(II) complexes reported here have lower angles and lower −J values, but clearly other geometric factors, reflected by τ_5, influence the strength of the interaction.

The literature presents numerous examples of monohydroxide-bridged compounds where the five-coordinate copper(II) is in square pyramidal geometry (Table 6). The magnitude of the antiferromagnetic coupling constant varies in a large interval, −J = 220 to 1146 cm^{-1}. More commonly, −J seems to adopt a value between 300 and 600 cm^{-1}. These data are in agreement with −J measured for **3**·2H$_2$O and **3**·1.5CH$_3$CN, 555 and 649 cm^{-1}, respectively. In the case of square pyramidal geometry significant superexchange interaction through the hydroxide bridge can be expected if the d$_{x^2-y^2}$ orbitals of copper(II) have the right orientation to overlap with the p$_x$ orbital of the hydroxide. For most examples with square pyramidal geometry, shown in Table 6, a change in the M–O–M angle (analogous to the in-plane rotation of the d$_{x^2-y^2}$ orbitals) would still result in significant overlap of these two orbitals (reflected by −J). The very large −J values (>1000 cm^{-1}) for some square pyramidal complexes[46–51] were explained by relatively large Cu–O–Cu angles, very short Cu–O bond lengths, and/or the cooperative effect of the hydroxide and other auxiliary ligands.

A characteristic feature of the spin Hamiltonian parameters of the copper(II) complexes studied here is the large E/D ratio, e.g., 0.62 in **6**·2H$_2$O.[52] The zfs parameters in dinuclear copper(II) complexes depend on exchange interactions in excited states of the dinuclear complex, in which one of the copper(II) ions is in its ground state, and the other is in an excited state, like $J_{x^2-y^2,xy}$ in the formulas shown below, which

Table 6. Structural and Magnetic Data ($\hat{H} = -J\hat{S}_1\hat{S}_2$) for Five-Coordinate Dicopper(II) Complexes with a Single Hydroxide Bridge

formula[a]	Cu···Cu (Å)	Cu−O−Cu (deg)	geometry[b]	τ_5	$-J$ (cm^{-1})	ref
[Cu$_2$(L^1)(OH)](ClO$_4$)$_3$·2H$_2$O	3.71	134.6	TBPeq	0.51	86	Asato[32]
[Cu$_2$(L^2)(OH)](ClO$_4$)$_2$·H$_2$O	3.03	103.7	SP	0.16/0.17	100	Neves[33]
[Cu$_2$(L^3)$_2$(OH)(ClO$_4$)(CH$_3$CN)]ClO$_4$	3.29	117.5	SP	0.15/0.08	220	Meyer[34]
[Cu$_2$(L^4)(OH)(ClO$_4$)]ClO$_4$	2.90	98.1	SP	0.19/0.34	238	Neves[33]
[Cu$_2$(L^5)(OH)(H$_2$O)(ClO$_4$)](ClO$_4$)$_2$	3.57	141.7	SP	0.26	240	Drew[35]
[Cu$_2$(L^6)(OH)(NO$_3$)$_2$(H$_2$O)$_2$]NO$_3$	3.10	109.3	SP	0.04/0.18	308	Thompson[36]
[Cu$_2$(L^7)$_4$(OH)](ClO$_4$)$_3$	3.65	141.6	TBPeq/SP	0.71/0.32	322	Hendrickson[37]
[Cu$_2$(L^8)$_2$(OH)](ClO$_4$)$_3$	3.66	139.8	SP	0.17	330	Spiccia[38]
[Cu$_2$(L^9)(dpm)(OH)](ClO$_4$)$_3$·2H$_2$O	3.66	137.9	SP	0.14	365[c]	Spodine[39]
[Cu$_2$(L^{10})(OH)(NO$_3$)(H$_2$O)](NO$_3$)·2H$_2$O	3.28	117.5	SP	0.30/0.33	395	Thompson[40]
[Cu$_2$(L^{11})(OH)(CF$_3$SO$_3$)(BPh$_4$)$_2$	3.89	166.1	SP	0.10/0.13	430	Nelson[41]
[Cu$_2$(L^{10})(OH)(H$_2$O)$_2$](ClO$_4$)$_2$·H$_2$O	3.31	117.9	SP	0.14/0.11	443	Thompson[40]
[Cu$_2$(L^{12})(OH)](ClO$_4$)$_3$·1.5H$_2$O	3.74[d]	150.6[d]	SP	0.16[d]	510	Adams[42]
[Cu$_2$(L^{13})(OH)(H$_2$O)](ClO$_4$)$_2$	3.01	102.9	SP/SPl	0.05	529	Kitagawa[43]
[Cu(L^{14})(L^{15})(OH)](ClO$_4$)·H$_2$O	3.57	138.2	SP	0.003	550	Spiccia[44]
[Cu$_2$(L$_m$)$_2$(OH)](ClO$_4$)$_3$·2H$_2$O (3·2H$_2$O)	3.87	141.0	SP	0.29/0.30	560	this work
[Cu$_2$(L$_m$)$_2$(OH)](ClO$_4$)$_3$·1.5CH$_3$CN (3·1.5CH$_3$CN)	3.64	141.2/151.0	SP	0.42/0.40	649	this work
[Cu$_2$(L^{16})(OH)](ClO$_4$)$_3$·H$_2$O	3.76	156.0	TBPax	0.83	691	Reedijk[30]
[Cu$_2$(L^{17})$_2$(OH)](ClO$_4$)$_3$	3.64	136.5	TBPax	0.66	760	Duan[45]
[Cu(L^{18})Br]$_2$(OH)(pz)	3.38	123.9	SP	0.26/0.42	770	Escrivà[46]
[Cu$_2$(L^{19})(OH)](ClO$_4$)$_3$·CH$_3$CN	3.76	155.6	TBPax/SP	0.83/0.42	795	Nelson[47]
[Cu$_2$(L$_m$*)$_2$(OH)](ClO$_4$)$_3$·2H$_2$O (5·2H$_2$O)	4.05	180.0	TBPeq	0.68	808	this work
[Cu$_2$(L^{20})(OH)](BF$_4$)$_3$	3.38	132.2	SP	0.13	850[c]	Osborn[48]
[Cu$_2$(L^{21})(OH)(CF$_3$SO$_3$)$_3$·H$_2$O	3.90	174.0	TBPax	0.88/0.95	865	Nelson[29]
[Cu$_2$(L^{22})(OH)(ClO$_4$)](ClO$_4$)$_2$·CHCl$_3$	3.64	143.7	SP	0.23	>1000	Lippard[49]
[Cu$_2$(L^{23})(OH)][ClO$_4$]$_2$·(CH$_3$)$_2$CO	3.53	136.7	SP	0.30/0.11	~1000	Wang[50]
[Cu$_2$(L^{24})(OH)](ClO$_4$)$_3$	3.39	123.0	SP/Oh	0.08	1146	Brooker[51]

[a]L^1 = 1,4,8,11-tetrakis(2-pyridylmethyl)-1,4,8,11-tetraazacyclotetradecane; L^2 = 6-amino-6-methylperhydro-1,4-diazepine; L^3 = 3,5-[3-bis(2-pyridyl)pyrazole-1-yl-methyl]pyrazole; L^4 = 2-[N,N-di(pyridine-2-ylmethyl)-aminomethyl]-4-methyl-6-[(6-methyl[1,4]diazepan-6-yl)iminomethyl]-phenol; L^5 = Shiff base of 2,6-diacetylpyridine and 3,6-dioxaoctane-1,8-diamine; L^6 = 1,4-bis(2-pyridylthio)phthalazine; L^7 = 2,2′-bipyridine; L^8 = 1-(2-guanidinoethyl)-1,4,7-triazacyclononane; L^9 = 1,1,2,2-tetrakis(2-pyridyl)ethylene, dpm = di(2-pyridyl)methane; L^{10} = N′3,N′6-dibenzylidenepyridazine-3,6-bis(carbohydrazonate); L^{11} = partially hydrolyzed Schiff base of 2,6-diacetylpyridine and tris(2-aminoethyl)amine, and tpmc = 1,4,8,11-tetrakis(2-pyridylmethyl)-1,4,8,11-tetraazacyclotetradecane; L^{12} = condensation of tris(2-aminoethyl)amine and 2,5-diformylfuran with Ba(ClO$_4$)$_2$; L^{13} = 2,6-bis[((4-imidazolylethyl)imino)methyl]-4-methylphenolate, L^{14} = 1,3-bis(1,4,7-triazacyclonon-1-ylmethyl)benzene; L^{15} = 4-nitrophenyl phosphate; L^{16} = 9,22-bis(pyridine-2′-ylmethyl) 1,4,9,14,17,22,27,28,29,30-decaazapentacyclo[22.2.1.^{4,7}1.^{11,14}1^{17,20}]triacontane 5,7(28),11(29),12,18,20(30),2(27),25-octaene; L^{17} = tris(2-aminoethyl)amine; L^{18} = 4-methoxy-2-(5-methoxy-3-methyl-1H-pyrazol-1-yl)-6-methylpyrimidine, pz = pyrazolate; L^{19} = 1,4,8,11,14,18,23,27-octaazabicyclo[9.9.9]nonacosane (amino-cryptand); L^{20} = 1,4-bis[(1-oxa-4,10-dithia-7-azacyclododecan-7-yl)methyl]benzene; L^{21} = condensation of tris(2-aminoethyl)amine and 2,5-diformylfuran; L^{22} = 1,4,7,13,16,19-hexaaza-10,22-dioxatetracosane; L^{23} = N,N′-bis(8-quinolylmethy1)-1,4,10,13-tetraoxa-7,16-diazacyclooctadecane; L^{24} = bis(pyridine-armed) acyclic Schiff base synthesized from 3,6-diformylpyridazine and two equivalents of 2-(2-aminoethyl)pyridine. [b]SP = square pyramidal (bridging O in equatorial position), TBPeq = trigonal bipyramidal with the bridge in an equatorial position, TBPax = trigonal bipyramidal with the bridge in an axial position, SPl = square planar; Oh = octahedral. [c]This value is an average of three runs. [d]This value is an average due to two independent cations in the unit cell.

were derived by Maurice et al. for the copper(II) paddlewheel complexes [copper(II) has a $d_{x^2-y^2}$ ground state].[53a]

$$D^{ex} = 2\frac{\xi^2 J_{x^2-y^2,xy}}{\Delta E^2_{x^2-y^2,xy}} - \frac{1}{4}\frac{\xi^2 J_{x^2-y^2,xz}}{\Delta E^2_{x^2-y^2,xz}} - \frac{1}{4}\frac{\xi^2 J_{x^2-y^2,yz}}{\Delta E^2_{x^2-y^2,yz}}$$

$$E^{ex} = \frac{1}{4}\frac{\xi^2 J_{x^2-y^2,xz}}{\Delta E^2_{x^2-y^2,xz}} - \frac{1}{4}\frac{\xi^2 J_{x^2-y^2,yz}}{\Delta E^2_{x^2-y^2,yz}} \qquad (7)$$

Note that all signs in eqs 7 were changed compared to the original formulas because the exchange Hamiltonian in ref 53a was written as $J\hat{S}_1\hat{S}_2$, while we use $-J\hat{S}_1\hat{S}_2$. ξ is the spin−orbit coupling constant for copper(II). An exchange interaction like $J_{x^2-y^2,xy}$ can contribute to the zfs only if there exists a nonzero matrix element of the angular momentum operator **L** between

corresponding metal orbitals, for example $\langle d_{x^2-y^2}|\mathbf{L}_z|d_{xy}\rangle = 2i$. This way, the spin−orbit coupling causes the exchange interactions to become anisotropic.

In the copper(II) paddlewheels, the Z axis is along the Cu···Cu direction, and the similarity of the arrangement of the d_{xz} and d_{yz} excited orbitals of one ion versus the ground $d_{x^2-y^2}$ orbital of another results in very small E values, so that $E/D <$ 0.03.[53] In our linear complexes, the Z and Y axes are perpendicular to Cu···Cu, while X is along that direction. The ground state in 6·2H$_2$O is d_{z^2}. Application of the technique described in ref 53a allows derivation of formulas for the exchange-related D and E parameters in this case:

$$D^{\text{ex}} = \frac{3}{4} \frac{\xi^2 J_{z^2,yz}}{\Delta E^2_{z^2,yz}} + \frac{3}{4} \frac{\xi^2 J_{z^2,xz}}{\Delta E^2_{z^2,xz}}$$

$$E^{\text{ex}} = -\frac{3}{4} \frac{\xi^2 J_{z^2,yz}}{\Delta E^2_{z^2,yz}} + \frac{3}{4} \frac{\xi^2 J_{z^2,xz}}{\Delta E^2_{z^2,xz}} \tag{8}$$

Formulas 8 are consistent with the exchange Hamiltonian written in the form $-J\hat{\mathbf{S}}_1\hat{\mathbf{S}}_2$. D^{ex} and E^{ex} depend on the sum and difference, respectively, of the two terms $\xi^2 J_{z^2,yz}/(\Delta E_{z^2,yz})^2$ and $\xi^2 J_{z^2,xz}/(\Delta E_{z^2,xz})^2$. The former one determines the magnitude of the anisotropic exchange-related zero-field splitting tensor component D^{ex}_{xx}, and the later one relates to D^{ex}_{yy}, while the D^{ex}_{zz} component must be 0. This is so because operator $\mathbf{L}_x$ has a nonzero matrix element between d_{z^2} and d_{yz}, $\mathbf{L}_y$ has a nonzero matrix element between d_{z^2} and d_{xz}, and all matrix elements of $\mathbf{L}_z$ between d_{z^2} and other d orbitals are 0. The X axis is the Cu···Cu direction and the Z axis is the trigonal bipyramid axis. The interactions between the d_{z^2} orbital of one ion and either d_{xz} or d_{yz} of another ion must be very different, considering different orientations in space of the d_{xz} or d_{yz} orbitals, resulting in large E^{ex} in this type of compound.[6] Formulas 8 show that if one of the $\xi^2 J_{z^2,yz}/(\Delta E_{z^2,yz})^2$ and $\xi^2 J_{z^2,xz}/(\Delta E_{z^2,xz})^2$ terms is much larger than the other one, then E^{ex} will be of approximately the same magnitude as D^{ex}. Interestingly, if the exchange interactions in the excited states described by $J_{z^2,yz}$ and $J_{z^2,xz}$ are ferromagnetic, that is, positive in our notation (which is expected since the overlap of d_{z^2} on one ion with d_{xz} or d_{yz} on another one is zero in linear M−O−M systems), then D^{ex} will be positive, opposite of the dinuclear copper carboxylates.[53a−d] Unfortunately, the sign of D could not be determined experimentally in this work. Its determination requires measuring high-field EPR spectra of single crystals at low temperatures,[53b,c] but this is not possible here owing to strong antiferromagnetism; when the temperature is lowered, the EPR spectra disappear before the D sign effect can manifest itself. That task is much simpler in ferromagnetic copper dimers, in which case powder HF EPR spectra are sufficient.[54] The Cu···Cu distance in 6·2H$_2$O is 4.05 Å, and the component of the dipolar zero-field interaction tensor[21] along that direction is $D^{\text{dip}}_{xx} = -0.03$ cm^{-1}, while $D^{\text{dip}}_{yy} = 0.015$ cm^{-1} and $D^{\text{dip}}_{zz} = 0.015$ cm^{-1}. From the experimental D and E parameters of 6·2H$_2$O (Table 3), assuming that they are positive (see above), one can calculate the components of the total zero-field splitting tensor, D_{xx}, D_{yy}, and D_{zz} of 0.064, −0.220, and 0.156 cm^{-1}, respectively. One can extract the exchange-related part of the zero field splitting tensor by subtracting the dipolar components from the total ones: $D^{\text{ex}}_{xx} = 0.094$ cm^{-1}, $D^{\text{ex}}_{yy} = -0.235$ cm^{-1}, and $D^{\text{ex}}_{zz} = 0.141$ cm^{-1}. A nonzero D^{ex}_{zz} is obtained because EPR always gives traceless zfs tensors. Subtracting 0.141 cm^{-1} from each of these components (which will not change the D and E magnitudes and signs; see SI) results in $D^{\text{ex}}_{xx} = -0.047$ cm^{-1}, $D^{\text{ex}}_{yy} = -0.376$ cm^{-1}, $D^{\text{ex}}_{zz} = 0$, or $D^{\text{ex}} = 0.164$ cm^{-1}, $E^{\text{ex}} = 0.211$ cm^{-1} (see eqs 8). The D^{ex}_{yy} component is related to the $J_{z^2,xz}$ interaction as explained above, which indeed should be stronger than $J_{z^2,yz}$. When assuming that the experimental D and E are negative, the above analysis leads to $D^{\text{ex}}_{xx} = 0.137$ cm^{-1}, $D^{\text{ex}}_{yy} = 0.376$ cm^{-1}, $D^{\text{ex}}_{zz} = 0$, or $D^{\text{ex}} = -0.256$ cm^{-1}, $E^{\text{ex}} = -0.119$ cm^{-1}. Negative D^{ex} is less plausible, as explained above. In any case, the zero-field splitting is clearly dominated by the anisotropic exchange interactions.

CONCLUSIONS

The first extensive series of metal complexes containing single hydroxide bridges with large M−O−M angles, ranging from 141° to exactly 180°, of the formulas [M$_2$(μ-OH)(μ-L$_m$)$_2$](ClO$_4$)$_3$ (M = Fe(II), Co(II), Cu(II)) and [M$_2$(μ-OH)(μ-L$_m$*)$_2$](ClO$_4$)$_3$ (M = Co(II), Ni(II), Cu(II)) have been prepared. As the M−O−M angle decreases, the geometry about the metal changes from distorted trigonal bipyramidal to more square pyramidal. The two cobalt(II) complexes show moderate antiferromagnetic coupling, $-J = 48-56$ cm^{-1}. The copper(II) complexes show strong antiferromagnetic coupling, $-J = 555-808$ cm^{-1}, where the exchange interactions were found to increase with the linearity of the Cu−O−Cu bridge and the d$_{z^2}$ character of the copper(II) ground state, a conclusion supported by DFT calculations. The EPR parameters of the copper(II) complexes show strong "rhombicity", which may be qualitatively understood by considering the interactions between the ground state of one copper(II) ion with the excited states of the other.

ASSOCIATED CONTENT

Ⓢ Supporting Information

X-ray crystallographic files in CIF format, additional information related to crystallographic studies and bond angles and lengths, fully labeled pictures of the dinuclear cationic units, electron density map near the hydroxide for 6·2H$_2$O, raw magnetic data for the copper complexes, g matrix orientation in 6, explanation of the zero-field splitting parameter conversion when changing the coordinate system. This material is available free of charge via the Internet at http://pubs.acs.org.

AUTHOR INFORMATION

Corresponding Authors
*Tel: 803-777-2587. Fax: 803-777-9521. E-mail: reger@mailbox.sc.edu.
*E-mail: ozarowsk@magnet.fsu.edu.

Notes
The authors declare no competing financial interest.

REFERENCES

(1) Selected reviews: (a) Chakrabarty, R.; Mukherjee, P. S.; Stang, P. J. *Chem. Rev.* **2011**, *111*, 6810. (b) Braga, D. J.; Brammer, L.; Champness, N. R. *CrystEngComm* **2005**, *7*, 1. (c) Zaworotko, M. J. *Cryst. Growth Des.* **2007**, *7*, 1740. (d) Zhao, D.; Timmons, D. J.; Yuan, D.; Zhou, H.-C. *Acc. Chem. Res.* **2011**, *44*, 123. (e) Chen, C.-L.; Zhang, J.-Y.; Su, C.-Y. *Eur. J. Inorg. Chem.* **2007**, 2997. (f) Northrop, B. H.; Yang, H.-B.; Stang, P. J. *Chem. Commun.* **2008**, *45*, 5896. (g) Lee, S. J.; Lin, W. *Acc. Chem. Res.* **2008**, *41*, 521. (h) Holliday, B. J.; Mirkin, C. A. *Angew. Chem., Int. Ed.* **2001**, *40*, 2022.
(2) Trofimenko, S. *J. Am. Chem. Soc.* **1970**, *92*, 5118.
(3) (a) Titze, C.; Hermann, J.; Vahrenkamp, H. *Chem. Ber.* **1995**, *128*, 1095. (b) Reger, D. L.; Grattan, T. C.; Brown, K. J.; Little, C. A.;

Lamba, J. J. S.; Rheingold, A. L.; Sommer, R. D. *J. Organomet. Chem.* **2000**, *607*, 120. (c) Vahrenkamp, H. *Acc. Chem. Res.* **1999**, *32*, 589. (d) Vahrenkamp, H. *Dalton Trans.* **2007**, 4751.

(4) (a) Reger, D. L.; Watson, R. P.; Gardinier, J. R.; Smith, M. D.; Pellechia, P. J. *Inorg. Chem.* **2006**, *45*, 10088. (b) Reger, D. L.; Foley, E. A.; Smith, M. D. *Inorg. Chem.* **2009**, *48*, 936.

(5) Reger, D. L.; Foley, E. A.; Watson, R. P.; Pellechia, P. J.; Smith, M. D.; Grandjean, F.; Long, G. J. *Inorg. Chem.* **2009**, *48*, 10658.

(6) (a) Reger, D. L.; Pascui, A. E.; Smith, M. D.; Jezierska, J.; Ozarowski, A. *Inorg. Chem.* **2012**, *51*, 11820. (b) Reger, D. L.; Pascui, A. E.; Smith, M. D.; Jezierska, J.; Ozarowski, A. *Inorg. Chem.* **2012**, *51*, 7966. (c) Reger, D. L.; Pascui, A. E.; Pellechia, P. J.; Smith, M. D. *Inorg. Chem.* **2013**, *52*, 11638.

(7) (a) Kahn, O. *Molecular Magnetism*; VCH Publishers, Inc.: New York, 1993. (b) Hay, P. J.; Thibeault, J. C.; Hoffmann, R. *J. Am. Chem. Soc.* **1975**, *97*, 4884.

(8) (a) Barrios, A. M.; Lippard, S. J. *J. Am. Chem. Soc.* **2000**, *122*, 9172. (b) Thomann, H.; Bernardo, M.; McCormick, J. M.; Pulver, S.; Andersson, K. K.; Lipscomb, J. D.; Salomon, E. I. *J. Am. Chem. Soc.* **1993**, *115*, 8881. (c) Yoon, J.; Fujii, S.; Solomon, E. I. *Proc. Natl. Acad. Sci.* **2009**, *106*, 6585. (d) Claus, H.; Decker, H. *Syst. Appl. Microbiol.* **2006**, *29*, 3. (e) Li, Y.; Wang, Y.; Jiang, H.; Deng, J. *Proc. Natl. Acad. Sci.* **2009**, *106*, 17002. (f) Gerdemann, C.; Eicken, C.; Krebs, B. *Acc. Chem. Res.* **2002**, *35*, 183. (g) Eicken, C.; Krebs, B.; Sacchetini, J. C. *Curr. Opin. Struct. Biol.* **1999**, *9*, 677. (h) Peisach, J.; Aisen, P.; Blumberg, W. E. *The Biochemistry of Copper*; Academic Press: New York, 1966.

(9) Hassan, A. K.; Pardi, L. A.; Krzystek, J.; Sienkiewicz, A.; Goy, P.; Rohrer, M.; Brunel, L.-C. *J. Magn. Reson.* **2000**, *142*, 300.

(10) (a) O'Connor, C. J. *Prog. Inorg. Chem.* **1982**, *29*, 203. (b) Bain, G. A.; Berry, J. F. *J. Chem. Educ.* **2008**, *85*, 532.

(11) (a) Barbour, L. J. *J. Supramol. Chem.* **2003**, *1*, 189. (b) POV-RAY 3.6, Persistence of Vision Raytracer Pty Ltd: Williamstown, Vic., Australia, 2006. (c) Laaksonen, L. *gOpenMol* version 3.00; www.csc.fi/english/pages/g0penMol.

(12) Wolsey, W. C. *J. Chem. Educ.* **1973**, *50*, A335−A337.

(13) *SMART* Version 5.630 and *SAINT+* Version 6.45; Bruker Analytical X-ray Systems, Inc.: Madison, WI, USA, 2003.

(14) *SADABS* Version 2.10; Bruker Analytical X-ray Systems, Inc.: Madison, WI, USA, 2003.

(15) *CellNow* and *TWINABS*; Bruker Analytical X-ray Systems, Inc.: Madison, WI, USA, 2003.

(16) (a) Sheldrick, G. M. *SHELXTL* Version 6.14; Bruker Analytical X-ray Systems, Inc.: Madison, WI, USA, 2000. (b) Sheldrick, G. M. *Acta Crystallogr.* **2008**, *A64*, 112.

(17) Dolomanov, O. V.; Bourhis, L. J.; Gildea, R. J.; Howard, J. A. K.; Puschmann, H. *J. Appl. Crystallogr.* **2009**, *42*, 339.

(18) Shannon, R. D. *Acta Crystallogr.* **1976**, *A32*, 751.

(19) Addison, A. W.; Rao, T. N.; Reedijk, J.; Van Rijn, J.; Verschoor, G. C. *J. Chem. Soc., Dalton Trans.* **1984**, 1349. $\tau_5 = (\beta - \alpha)/60°$ where α and β are the two largest angles measured around the metal centers. Perfect square pyramid: $\tau_5 = 0$; perfect trigonal bipyramid: $\tau_5 = 1$.

(20) (a) Telser, J.; Ozarowski, A.; Krzystek, J. *Electron Paramag. Reson.* **2013**, *23*, 209. (b) Zadrozny, J. M.; Long, J. R. *J. Am. Chem. Soc.* **2011**, *133*, 20732.

(21) (a) Abragam, A.; Bleaney, B. *Electron Spin Resonance of Transition Ions*; Clarendon Press: London, 1970. (b) Bencini, A.; Gatteschi, D. *EPR of Exchange Coupled Systems*; Springer-Verlag: Berlin, 1990.

(22) (a) Neese, F. *ORCA - An ab Initio, Density Functional and Semiempirical Program Package*, Version 2.9.1; 2012. (b) Neese, F. *Comput. Mol. Sci.* **2012**, *2*, 73.

(23) (a) Becke, D. A. *Phys. Rev. A* **1988**, *38*, 3098. (b) Perdew, J. P. *Phys. Rev. B* **1986**, *33*, 8822. (c) Perdew, J. P. *Phys. Rev. B* **1986**, *34*, 7406. (d) Kendall, R. A.; Früchtl, H. A. *Theor. Chem. Acc.* **1997**, *97*, 158.

(24) (a) Schaefer, A.; Horn, H.; Ahlrichs, R. *J. Chem. Phys.* **1992**, *97*, 2571. (b) Ahlrichs, R.; et al., unpublished results. The Ahlrichs auxiliary basis sets were obtained from the TurboMole basis set library under ftp.chemie.uni-karlsruhe.de/pub/jbasen.

(25) (a) Reinen, D.; Friebel, C. *Inorg. Chem.* **1984**, *23*, 791. (b) Arriortua, M. I.; Mesa, J. L.; Rojo, T.; Debaerdemaeker, T.; Beltrán-Porter, D.; Stratemeier, H.; Reinen, D. *Inorg. Chem.* **1987**, *27*, 2976. (c) Bianchi, A.; Fallani, D. G.; Ghilardi, C. A.; Sacconi, L. *J. Chem. Soc., Dalton Trans.* **1973**, 641.

(26) (a) Bersuker, I. B. *The Jahn−Teller Effect*; University Press: Cambridge, UK, 2006. (b) Harrison, D.; Kennedy, D.; Hathaway, B. *Inorg. Nucl. Chem. Lett.* **1981**, *17*, 87.

(27) Selected publications: (a) Shakya, R.; Powell, D. R.; Houser, R. P. *Eur. J. Inorg. Chem.* **2009**, 5319. (b) Drabent, K.; Ciunik, Z.; Ozarowski, A. *Inorg. Chem.* **2008**, *47*, 3358. (c) Ray, N. A.; Neves, A.; De Almeida, W. B.; Dos Santos, H. F.; Costa, L. A. S. *Int. J. Quantum Chem.* **2010**, *110*, 1432. (d) Wikstrom, J. P.; Filatov, A. S.; Mikhalyova, E. A.; Shatruk, M.; Foxman, B. M.; Rybak-Akimova, E. V. *Dalton Trans.* **2010**, *39*, 2504. (e) Wang, L.; Lu, S.; Zhou, Y.; Guo, X.; Lu, Y.; He, J.; Evans, D. G. *Chem. Commun.* **2011**, *47*, 11002. (f) Curtis, N. F.; Morgan, K. R.; Rickard, C. E. F.; Waters, J. M. *Polyhedron* **2010**, *29*, 1279. (g) Manzur, J.; Vega, A.; Garcia, A. M.; Acuña, C.; Sieger, M.; Sarkar, B.; Niemeyer, M.; Lissner, F.; Schleid, T.; Kaim, W. *Eur. J. Inorg. Chem.* **2007**, 5500. (h) Bruijnincx, P. C. A.; Buurmans, I. L. C.; Huang, Y.; Juhász, G.; Viciano-Chumillas, M.; Quesada, M.; Reedijk, J.; Lutz, M.; Spek, A. L.; Münck, E.; Bominaar, E. L.; Klein Gebbink, R. J. M. *Inorg. Chem.* **2011**, *50*, 9243. (i) Graham, B.; Hearn, M. T. W.; Junk, P. C.; Kepert, C. M.; Mabbs, F. E.; Moubaraki, B.; Murray, K.; Spiccia, L. *Inorg. Chem.* **2001**, *40*, 1536. (j) Incarvito, C.; Rheingold, A. L.; Gavrilova, A. L.; Qin, C. J.; Bosnich, B. *Inorg. Chem.* **2001**, *40*, 4101. (k) Plieger, P. J.; Downard, A. J.; Moubaraki, B.; Murray, K. S.; Brooker, S. *Dalton Trans.* **2004**, 2157. (l) He, C.; Lippard, S. J. *J. Am. Chem. Soc.* **2000**, *122*, 184. (m) Melnik, M. *Coord. Chem. Rev.* **1982**, *42*, 259. (n) Tanase, S.; van Son, M.; van Albada, G. A.; de Gelder, R.; Bouwman, E.; Reedijk, J. *Polyhedron* **2006**, *25*, 2967. (o) Gutierrez, L.; Alzuet, G.; Real, J. A.; Cano, J.; Borrás, J.; Casteñieras, A. *Inorg. Chem.* **2000**, *39*, 3609. (p) Prescimone, A.; Sanchez-Benitez, J.; Kamenev, K. K.; Moggach, S. A.; Warren, J. E.; Lennie, A. R.; Murrie, M.; Parsons, S.; Brechin, E. K. *Dalton Trans.* **2010**, *39*, 113. (q) References from Table 6.

(28) (a) Evans, D. R.; Mathur, R. S.; Heerwegh, K.; Reed, C. A.; Xie, Z. *Angew. Chem., Int. Ed.* **1997**, *36*, 1335. (b) Cheng, B.; Fries, P. H.; Marchon, J.-C.; Scheidt, W. R. *Inorg. Chem.* **1996**, *35*, 1024. (c) Scheidt, W. R.; Cheng, B.; Safo, M. K.; Cukiernik, F.; Marchon, J.-C.; Debrunner, P. G. *J. Am. Chem. Soc.* **1992**, *114*, 4420.

(29) (a) Lu, Q.; Latour, J. -M.; Harding, C. J.; Martin, N.; Marrs, D. J.; McKee, V.; Nelson, J. *J. Chem. Soc., Dalton Trans.* **1994**, 1471. (b) Harding, C. J.; McKee, V.; Nelson, J.; Lu, Q. *J. Chem. Soc., Dalton Trans.* **1993**, 1768.

(30) Koval, I. A.; van der Schilden, K.; Schuitema, A. M.; Gamez, P.; Belle, C.; Pierre, J.; Lüken, M.; Krebs, B.; Roubeau, O.; Reedijk, J. *Inorg. Chem.* **2005**, *44*, 4372.

(31) Patra, A.; Ray, M.; Mukherjee, R. *Polyhedron* **2000**, 1423.

(32) Asato, E.; Toftlund, H.; Kida, S. *Inorg. Chim. Acta* **1989**, *165*, 207.

(33) Rey, N. A.; Neves, A.; Bortoluzzi, A. J.; Haase, W.; Tomkowicz, Z. *Dalton Trans.* **2012**, *41*, 7196.

(34) Singh, A. K.; van der Vlugt, J. I.; Demeshko, S.; Dechert, S.; Meyer, F. *Eur. J. Inorg. Chem.* **2009**, 3431.

(35) Drew, M. G. B.; McCann, M.; Martin-Nelson, M. *J. Chem. Soc., Dalton Trans.* **1981**, 1868.

(36) Chen, L.; Thompson, L. K.; Bridson, J. N. *Inorg. Chem.* **1993**, *32*, 2938.

(37) Haddad, M. S.; Wilson, S. R.; Hodgson, D. J.; Hendrickson, D. N. *J. Am. Chem. Soc.* **1981**, *103*, 384.

(38) Tjioe, L.; Joshi, T.; Forsyth, C. M.; Moubraki, B.; Murray, K. S.; Brugger, J.; Graham, B.; Spiccia, L. *Inorg. Chem.* **2012**, *51*, 939.

(39) Spodine, E.; Manzur, J.; Garland, M. T.; Kiwi, M.; Peña, O.; Grandjean, D.; Toupet, L. *J. Chem. Soc., Dalton Trans.* **1991**, 365.

(40) Dey, S. K.; Abedin, T. S. M.; Dawe, L. N.; Tandon, S. S.; Collins, J. L.; Thompson, L. K.; Postnikov, A. V.; Alam, M. S.; Müller, P. *Inorg. Chem.* **2007**, *46*, 7767.

(41) Harding, C. J.; Lu, Q.; Malone, J. F.; Marrs, D. J.; Martin, N.; McKee, V.; Nelson, J. *J. Chem. Soc., Dalton Trans.* **1995**, 1739.

(42) Adams, H.; Bailey, N. A.; Collinson, S. R.; Fenton, D. E.; Harding, C. J.; Kitchen, S. J. *Inorg. Chim. Acta* **1996**, *246*, 81.

(43) Maekawa, M.; Kitagawa, S.; Munakata, M.; Masuda, H. *Inorg. Chem.* **1989**, *28*, 1904.

(44) Fry, F. H.; Spiccia, L.; Jensen, P.; Moubaraki, B.; Murray, K. S.; Tieknik, E. R. T. *Inorg. Chem.* **2003**, *42*, 5594.

(45) Duan, C.-y.; Lu, Z.-l; You, X.-z. *Trans. Met. Chem.* **1998**, *23*, 77.

(46) Escrivà, E.; García-Lozano, J.; Martínez-Lillo, J.; Nuñez, H.; Server-Carrió, J.; Soto, L.; Carrasco, R.; Cano, J. *Inorg. Chem.* **2003**, *42*, 8328.

(47) Chin, A.; Edgar, M.; Harding, C. J.; McKee, V.; Nelson, J. *Dalton Trans.* **2009**, 6315.

(48) Burk, P. L.; Osborn, J. A.; Youinou, M. *J. Am. Chem. Soc.* **1981**, *103*, 1273.

(49) Coughlin, P. K.; Lippard, S. J. *J. Am. Chem. Soc.* **1981**, *103*, 3228.

(50) Wang, D.; Xiang, H.; Wang, G.; Han, Z.; Yang, X.; Hu, H.; Yu, K. *J. Chem. Soc., Dalton Trans.* **1994**, 3325.

(51) Plieger, P. G.; Downard, A. J.; Moubaraki, B.; Murray, K. S.; Brooker, S. *Dalton Trans.* **2004**, 2157.

(52) D and E values reported here refer to the system of coordinates in which the Z direction is along the trigonal bipyramid axis. It is possible to convert them to obey the convention $E \leq D/3$ by renaming the coordinate axes (see SI).

(53) (a) Maurice, R.; Sivalingam, K.; Ganyushin, D.; Guihery, N.; de Graaf, C.; Neese, F. *Inorg. Chem.* **2011**, *50*, 6229. (b) Ozarowski, A. *Inorg. Chem.* **2008**, *47*, 9760. (c) Ozarowski, A.; Szymanska, I. B.; Muziol, T.; Jezierska, J. *J. Am. Chem. Soc.* **2009**, *131*, 10279. (d) Reger, D. L.; Debreczeni, A.; Smith, M. D.; Jezierska, J. *Inorg. Chem.* **2012**, *51*, 1068.

(54) Sharma, R. P.; Saini, A.; Monga, D.; Venugopalan, P.; Jezierska, J.; Ozarowski, A.; Ferretti, V. *New J. Chem.* **2014**, *38*, 437.

1988

dx.doi.org/10.1021/ic4017905 | *Inorg. Chem.* 2014, 53, 1975−1988